coatings

MDPI

Article

Comprehensive Evaluation of 45S5 Bioactive Glass Doped with Samarium: From Synthesis and Physical Properties to Biocompatibility and Antimicrobial Activity

Maxim V. Maximov [1,2,3,4,5,6], Oana Cristina Maximov [2], Ludmila Motelica [3,4,5,6], Denisa Ficai [3,4,5,6,7], Ovidiu Cristian Oprea [3,4,5,6,7], Roxana Doina Trușcă [1,3,4,5,6], Liliana-Roxana Balahura (Stămat) [8], Radu Pericleanu [9], Andreea Ștefania Dumbravă [9], Viorica Maria Corbu [10,11], Vasile-Adrian Surdu [1,12], Gabriel Vasilievici [13], Anton Ficai [1,3,4,5,6,*], Sorina Dinescu [8,11,†] and Irina Gheorghe-Barbu [9,11,†]

1 Science and Engineering of Oxide Materials and Nanomaterials, Faculty of Chemical Engineering and Biotechnology, National University of Science and Technology POLITEHNICA Bucharest, Gh. Polizu 1-7, 011061 Bucharest, Romania; maxim.maximov88@yahoo.com (M.V.M.); truscaroxana@yahoo.com (R.D.T.); adrian.surdu@upb.ro (V.-A.S.)
2 Microsin, Pericle Papahagi st., No 51-63, 032364 Bucharest, Romania; oana_cristina_duta@yahoo.com
3 National Research Center for Food Safety, National University of Science and Technology POLITEHNICA Bucharest, Splaiul Independentei 313, 060042 Bucharest, Romania; motelica_ludmila@yahoo.com (L.M.); denisaficai@yahoo.ro (D.F.); ovidiu73@yahoo.com (O.C.O.)
4 National Center for Micro and Nanomaterials, National University of Science and Technology POLITEHNICA Bucharest, Splaiul Independentei 313, 060042 Bucharest, Romania
5 Academy of Romanian Scientists, Ilfov Street 3, 050044 Bucharest, Romania
6 CAMPUS Centre, National University of Science and Technology POLITEHNICA Bucharest, Splaiul Independentei 313, 060042 Bucharest, Romania
7 Department of Inorganic Chemistry, Physical Chemistry and Electrochemistry, Faculty of Chemical Engineering and Biotechnology, National University of Science and Technology POLITEHNICA Bucharest, Gh. Polizu 1-7, 011061 Bucharest, Romania
8 Department of Biochemistry and Molecular Biology, University of Bucharest, 050095 Bucharest, Romania; roxana.balahura@bio.unibuc.ro (L.-R.B.); sorina.dinescu@bio.unibuc.ro (S.D.)
9 Department of Botany and Microbiology, Faculty of Biology, University of Bucharest, Intr. Portocalelor No. 1–3, 060101 Bucharest, Romania; radu.pericleanu@s.unibuc.ro (R.P.); dumbrava.andreea-stefania22@s.bio.unibuc.ro (A.Ș.D.); irina.gheorghe@bio.unibuc.ro (I.G.-B.)
10 Department of Genetics, Faculty of Biology, University of Bucharest, Intr. Portocalelor No. 1–3, 060101 Bucharest, Romania; viorica-maria.corbu@bio.unibuc.ro
11 The Research Institute of the University of Bucharest (ICUB), B.P Hasdeu No. 7, 050095 Bucharest, Romania
12 Department of Materials Science, Faculty of Materials Science and Engineering, Transilvania University of Brasov, 29 Eroilor Blvd., 500036 Brasov, Romania
13 National Institute for Research & Development in Chemistry and Petrochemistry-ICECHIM Bucharest, 202 Spl. Independentei, 6th District, 060021 Bucharest, Romania; gabi.vasilievici@gmail.com
* Correspondence: anton.ficai@upb.ro
† These authors have equal contributions and share the last author position.

check for updates

Academic Editors: Rafael Comesaña and Gabriela Ciobanu

Received: 21 February 2025
Revised: 21 March 2025
Accepted: 26 March 2025
Published: 28 March 2025

Citation: Maximov, M.V.; Maximov, O.C.; Motelica, L.; Ficai, D.; Oprea, O.C.; Trușcă, R.D.; Balahura, L.-R.; Pericleanu, R.; Dumbravă, A.Ș.; Corbu, V.M.; et al. Comprehensive Evaluation of 45S5 Bioactive Glass Doped with Samarium: From Synthesis and Physical Properties to Biocompatibility and Antimicrobial Activity. *Coatings* **2025**, *15*, 404. https://doi.org/10.3390/coatings15040404

Abstract: This paper describes the synthesis and evaluation of samarium-doped 45S5 bioactive glass in various ratios. The bioactive glass samples were prepared using the sol–gel method and subjected to a heat treatment at 700 °C in normal atmosphere. The obtained samples were analyzed by thermogravimetric analysis (TGA) before and after the heat treatment to assess their thermal stability and compositional changes. The bioactivity of the samples was tested in vitro by immersion in simulated body fluid (SBF) at 36.5 ± 0.5 °C (normal human body temperature) and pH 7.4 (the pH of the human blood plasma), for several time periods. During the test, the pH and conductivity of the SBF solutions were monitored to track ion migration. After the in vitro test, the mass loss was evaluated and the formation of hydroxycarbonate apatite (HCA) was analyzed by FTIR spectroscopy. The microstructure of the bioactive glasses was examined using scanning electron microscopy (SEM) and the density of bioactive glass was also determined using Archimedes' principle. This study also investigated the antimicrobial and anti-biofilm properties of both undoped

and samarium-doped 45S5 bioactive glass through qualitative and quantitative assays against a range of microorganisms, including Gram-negative, Gram-positive, and yeast reference strains. The results were compared with literature data on melt-derived bioactive glass to evaluate the effects of Sm doping and the sol–gel synthesis method on bioactive glass performance.

Keywords: bioactive glass 45S5; sol–gel synthesis; samarium-doped bioactive glass; in vitro evaluation; anti-biofilm; virulence factor modulation

1. Introduction

In 1969, professor Larry Hench developed the first bioactive glass (BG), named 45S5. Currently, this biomaterial has a multitude of applications in the biomedical field [1]. For example, bioactive glass is used for bone replacement, bone tissue regeneration, and soft tissue engineering [2]. Moreover, the use of these materials in combination with modern technologies enables the fabrication of advanced biodevices for bone implants [3]. Their preparation can be achieved via two methods: melt-derived BG and the sol–gel method. Each method has its advantages and disadvantages, but it is generally considered that glass obtained by the sol–gel method is more reactive over a wider range of compositions due to its unique textural properties (inherent nanoporosity) [4]. In addition, it was demonstrated that the degree of crystallinity and the bioactivity of the obtained glasses can change depending on the thermal treatment applied during the preparation process [5].

Bone tissue engineering is a field of great interest due to the numerous bone malformations and pathologies encountered in patients of various ages. Bioactive glasses are used in numerous medical applications due to their high biocompatibility, antibacterial properties, and functional characteristics [6]. Advanced experiments revealed the beneficial influence of the bioactive glasses on osteogenesis, considering their capacity to stimulate HCA formation and cells' adhesion and proliferation [7]. Moreover, being class A bioactive materials, 45S5 bioactive glasses promote the osteoblast metabolism and secretion of growth factors, thus enhancing the reconstruction of bone tissue [8]. In recent years, numerous bioactive compounds have been studied to improve the osteogenic properties and biocompatibility of bioactive glasses. Lanthanides, such as cerium or samarium, represent promising candidates for bone tissue engineering due to their high affinity for bone structure, specificity for Ca^{2+} sites, and antibacterial and osteogenic properties [9].

Doping bioactive glasses with ions can change the therapeutic effect of the biomaterial and can also influence the structure and processing method. Apart from the "classic" elements, recently more "exotic" ions have been used for doping. It has been observed that these elements can enhance the biological and physical performance of bioactive glasses, giving anti-inflammatory, antibacterial, fluorescence, and luminescence properties [10]. This luminescence facilitates non-destructive, real-time imaging and tracking of the implants within the body, enhancing the monitoring of implant integration and tissue regeneration. One of these studied rare elements is samarium. Samarium has no biological role, but shows an increased affinity for bone tissue; it can be located in the skeleton and in areas of increased bone turnover [11]. Bioactive glass doped with samarium exhibits photoluminescence and fluorescence [12]. Additionally, the addition of 2 mol% Sm_2O_3 to a bioglass–hydroxyapatite composite decreases the degree of adhesion of *Staphylococcus aureus* and *Staphylococcus epidermidis*, thus conferring antibacterial properties to the obtained composite; in addition to that, there was observed a proliferation of MG63 cells [9,13]. In vitro biological assessments indicate that samarium-doped hydroxyapatite nanoparticles are biocompatible with the MC3T3-E1 preosteoblast cell line and sustain their

osteogenic activity [14]. Sm/Ag-doped bioactive glass promotes mineralization and has significant antibacterial capabilities [15]. Samarium has also been tested for other types of applications, such as the preparation of microspheres from mesoporous bioactive glass with applications in drug delivery. The results showed that the rate of drug release is proportional to the amount of samarium used for doping [16]. Samarium radionuclide 153Sm (β-decay, half-life 1.9 days) is used for the treatment of bone cancer, prostate cancer [17–19], breast cancer metastatic to the bone, elapsed or refractory multiple myeloma, and bone pain [11]. Due to the short emission distance in the bone (1.7 mm), the radiation exposure of the bone marrow and adjacent tissues is limited [20,21].

Although samarium is a well-studied element, its use as a doping agent for bioactive glass remains relatively less explored. Given the outlined objectives, we aim to comprehensively characterize the physicochemical properties of 45S5 bioactive glass, both in its undoped form and doped with samarium. Additionally, we will evaluate their biocompatibility, antimicrobial activity, anti-biofilm efficacy, and potential to modulate virulence factors. These investigations will help to explore the potential applications of these materials in bone tissue engineering as well as other biomedical fields.

2. Materials and Methods

In the experiments performed, the following reagents were used: tetraethyl orthosilicate (TEOS; 99.9%) from VWR (Radnor, PA, USA), triethyl phosphate (TEP; 99%), nitric acid (65%), tris(hydroxymethyl) aminomethane (TRIS; 99%), acetone (99.8%), and hydrochloric acid (37%), all from Merck (Darmstadt, Germany); calcium nitrate tetrahydrate (99%), samarium nitrate hexahydrate (99.9%), sodium chloride (99%), and calcium chloride dihydrate (99%), all from Sigma-Aldrich (St. Louis, MO, USA); sodium nitrate (99.5%), potassium chloride (99%), sodium bicarbonate (99%), potassium phosphate dibasic (99%), and sodium sulfate (99%), all from SILAL (Bucharest, Romania); and magnesium chloride hexahydrate (99%) from Fluka (Charlotte, NC, USA).

The MC3T3-E1 cell line (CRL-2593) was purchased from ATCC, Manassas, VA, USA. Dulbecco Modified Eagle's Medium (DMEM) low glucose, antibiotic antimycotic solution, phosphate buffered saline (PBS) powder, 3-(4,5-dimethylthiazolyl-2)-2,5-diphenyltetrazolium bromide (MTT) reagent, and "in vitro toxicology assay kit lactate dehydrogenase (LDH) based" (TOX7-1KT) assay kit were purchased from Sigma-Aldrich, Germany. Fetal bovine serum (FBS) and the Live/Dead assay kit were purchased from Thermo Fisher Scientific, Waltham, MA, USA.

2.1. Bioactive Glass Preparation

Bioactive glass with a mass ratio of SiO_2:P_2O_5:CaO:Na_2O as 45%:6%:24.5%:24.5% and a molar ratio of 46.1%:2.6%:26.9%:24.4%, which corresponds to the composition of 45S5 bioactive glass, was prepared using the sol–gel method according to the procedure described below. In a 250 mL three-necked round-bottom flask, equipped with a mechanical stirrer, thermometer, and an addition funnel with pressure equalization, 75 g (4.16 mol) demineralized water and 2 mL HNO_3 (2N) were introduced. The water:TEOS ratio was 25:1. The resulting solution was warmed to 40 °C ± 5 °C. A certain amount of tetraethyl orthosilicat, 39 g (0.187 mol), was introduced into the reaction mass using a dropping funnel over ~1.5 h. After the addition of TEOS, the reaction mass was stirred for 30 min, then 3.85 g (0.0211 mol) of triethyl phosphate was added over a period of 10 min. The resulting mixture was stirred for an additional 30 min. Then, 25.8 g (0.109 mol) of calcium nitrate tetrahydrate was added in portions of 2 g, each portion being added after the previous portion was dissolved. After the complete addition of calcium nitrate, the reaction mass was stirred for

15 min, after which 16.8 g (0.198 mol) of sodium nitrate was added in portions of 2 g; each portion was added after the complete dissolution of the previous portion.

The bioactive glasses doped with +0.1, +1.0, and +3.0% wt samarium were prepared using the same synthesis process, with the difference that after the addition of nitrate, 0.075 g, 0.75 g, and 2.25 g of samarium nitrate hexahydrate, respectively, was added to the reaction mass, according to Table 1. After adding all the components, the reaction mass was stirred for another 24 h at 25 °C ± 5 °C and then left to rest for 7 days. The formed gel was transferred to alumina crucible, grinded, and dried at 130 °C for 8 h. The resulting powder was heat-treated at 700 °C at a rate of 5 °C/min, then held for 3 h at 700 °C, after which it was cooled and crushed again using a mortar. In each experiment, 24.5–25.5 g of white powder was obtained, which corresponds to a yield of 98%.

Table 1. Samarium nitrate quantities added in the samples of bioactive glass.

Name	Quantity $Sm(NO_3)_3*6H_2O$ (g)	Sm (Mass %)
45S5	-	-
45S5 + 0.1% Sm	0.075 g	0.1%
45S5 + 1.0% Sm	0.75 g	1.0%
45S5 + 3.0% Sm	2.25 g	3.0%

2.2. Thermogravimetric Measurements

Thermal behavior was followed with a STA 449C F3 system, TG-DSC (thermogravimetry–differential scanning calorimetry) from Netzsch (NETZSCH-Gerätebau GmbH, Selb, Germany), between 20–900 °C, with a sample heating rate of 10 °C/min, in dynamic (50 mL/min) air atmosphere.

2.3. SEM Microscopy

The morphology of the obtained surface was analyzed using a QUANTA INSPECT F50 scanning electron microscope (FEI, Eindhoven, The Netherlands) equipped with a field emission gun with a resolution of 1.2 nm and an energy dispersive X-ray spectrometer with a MnK resolution of 133 eV.

2.4. X-Ray Diffraction Analysis

Phase composition was investigated using a PANalytical Empyrean X-ray diffractometer (Cedar Park, TX, USA) operated in theta–theta geometry. The instrument was equipped with a CuKα (λ = 1.5418 Å) sealed X-ray tube, featuring a fixed 1/4° divergence slit and a 1/2° anti-scatter slit on the incident beam side. On the diffracted beam side, it included a 1/2° anti-scatter slit and a Ni-filter mounted on a PIXcel3D detector operated in 1D mode. Analyses were conducted over a 2θ range of 5–80° with a step size of 0.026°, a counting time per step of 255 s, and a revolution time of 1 s. The recorded patterns were indexed using HighScore Plus 3.0.e software in conjunction with the Crystallography Open Database (COD). Phase quantification was performed by Rietveld refinement, utilizing a polynomial function for background approximation, a pseudo-Voigt function for peak profile fitting, and a Caglioti function for peak width determination.

2.5. Density Determination and BET Analysis

The density of the bioglass samples was determined using the Archimedes principle. For this, 0.5 g of crushed bioactive glass powder was weighed, over which a pressure of 250 MPa was applied, under vacuum, resulting, in the end, in discs with a diameter of 10 mm. The determination of the density of the obtained samples was carried out

using demineralized water as immersion solvent. All measurements were performed 3 times for each type of bioactive glass at 23 °C using an analytical balance (RADWAG 0.0000g, Model AS 220.R2), and the average value was determined (as well as the standard deviation ± SD).

Textural characteristics of the bioactive glasses (surface area, pore volume, and average pore diameter) were determined on an Autosorb 1 Nova 2200 Analyzer (Quantacrome Instruments, Boynton Beach, FL, USA). Texture data were obtained by the automatic recording and processing of adsorption–desorption isotherms of nitrogen. The specific surface area was calculated using the equation in the linear part of the BET adsorption isotherm. To assess the pore size, the desorption branch of isotherms with hysteresis was used by applying the BJH method.

2.6. Bioactivity Evaluation In Vitro

In order to evaluate in vitro bioactivity of bioactive glasses obtained, a mass of ~0.5 g bioactive glass was weighed with an accuracy of 0.0001 g, in polyethylene containers, with lids. In every sample, 50 mL of simulated body fluid (SBF) solution (pH = 7.40, solution prepared according to the procedure described by Kokubo and Takadama [22]) was added. In Table 2, the concentrations of ions present in the SBF solution are listed. The suspensions obtained were kept at 36.5 °C ±0.5 °C for 1, 3, 7, 14, and 21 days, respectively, occasionally stirring the contents of the containers. The experiments were performed for all the prepared samples and were repeated 3 times. The values presented in this paper are the average values obtained.

Table 2. Ion concentration (mM/L) in SBF and in human blood plasma.

Ions	Na^+	K^+	Ca^{2+}	Mg^{2+}	HCO_3^-	Cl^-	HPO_4^{2-}	SO_4^{2-}
SBF	142	5.0	2.5	1.5	4.2	148	1.0	0.5
Human blood plasma	142	5.0	2.5	1.5	27.0	103	1.0	0.5

2.7. Determination of pH Variation, Ionic Strength, and Mass Loss

After immersing the bioactive glasses in SBF for the specified time periods, the samples were vacuum filtered. The pH and conductivity of the filtrate was measured at 33–34 °C using a Multi 9630 IDS apparatus equipped with pH and conductance electrodes. The filtered powders were washed with 3 × 15 mL of demineralized water, then with 3 × 10 mL of acetone, dried at 105 °C for 1 h, and then weighed on the analytical balance (RADWAG 0.0000g, Model AS 220.R2). The obtained results were compared with the initial masses of the samples.

2.8. Biocompatibility Test

2.8.1. Cell Culture Model

The preosteoblast MC3T3-E1 cell line was used in order to observe the effect of the 45S5 bioactive glasses doped with different concentrations of samarium. MC3T3-E1 cells were cultured in DMEM media supplemented with 10% FBS and 1% antibiotic antimycotic solution and maintained at 37 °C, 5% CO_2, in a humidified atmosphere. The cell culture was propagated for many passages, and when confluent, the cells were seeded at a density of 2.5×10^4 cells/cm^2 in triplicate in a 48-well plate and incubated in standard conditions for 24 h in order to allow cell attachment to the surface.

For the indirect experiments, the 45S5 bioactive glasses doped with 0.1% Sm, 1% Sm, and 3% Sm were sterilized and incubated in DMEM media for 24 h at 37 °C. The conditioned media of 45S5, 45S5 + 0.1% Sm, 45S5 + 1% Sm, and 45S5 + 3% Sm were

put in contact with the preosteoblasts seeded in a 48-well plate and incubated in standard culture conditions for additional 24 and 48 h. The culture plates were regularly observed with a phase contrast microscope.

2.8.2. Biocompatibility Assays

In order to evaluate the biocompatibility of the enriched 45S5 bioactive glasses, viability and cytotoxicity assays were performed at 24 and 48 h after the conditioned media addition. Cell viability profile was determined using a qualitative Live/Dead fluorescent staining and quantitative MTT assay, while the glasses' cytotoxicity was determined using a LDH assay.

2.8.3. Live/Dead Assays

Live/Dead fluorescent staining was performed in order to observe the ratio between the live cells and dead cells. The staining solution was prepared according to the manufacturer's instructions and incubated with the samples for one hour in dark conditions. The visualization of live cells and dead cells' nuclei was performed employing an Olympus IX73 (Olympus, Tokyo, Japan) microscope equipped with a Hamamatsu ORCA-03G camera (A3472-06, Hamamatsu, Japan) and the images were acquired using CellSens Dimension software (v1.11, Olympus).

2.8.4. MTT Assay

The preosteoblasts' viability was quantitatively measured using a spectrophotometric MTT (3-(4,5-dimethylthiazolyl-2)-2,5-diphenyltetrazolium bromide) assay. The cell cultures were incubated with 1 mg/mL MTT solution for 4 h, allowing the formation of formazan crystals by the metabolic active cells. The formazan crystals were solubilized with isopropanol and the optic density was measured at 550 nm on a Flex Station 3 (Molecular Devices, San Jose, CA, USA). The values obtained were directly proportional with the amount of live cells.

2.8.5. LDH Assay

The cytotoxic potential of the enriched 45S5 bioactive glasses was determined using an "In vitro toxicology assay kit lactate dehydrogenase (LDH) based" TOX7 kit. The culture media was collected from the culture wells, mixed with the components of the kit, and incubated in the dark and at room temperature for 10–15 min, according to the manufacturer's instructions. The optical density was measured by spectrophotometry at 490 nm on the Flex Station 3. The values obtained were directly proportional with the amount of dead cells.

2.8.6. Statistical Analysis

All tests were performed in triplicate. Statistical analysis of the data was performed using GraphPad 9 Prism software, the one-way ANOVA method, and the Bonferroni post-test, taking as statistically significant a p value < 0.05.

2.9. Antimicrobial and Anti-Biofilm Properties and the Influence of 45S5 Bioactive Glass on the Soluble Virulence Factors' Modulation

2.9.1. Qualitative Screening of 45S5 Bioactive Glass Against Reference Microbial Strains

This study utilized a modified diffusion assay to assess the antimicrobial activity of 45S5 bioactive glass, both undoped and doped with samarium at various concentrations (0.1%, 1.0%, and 3.0%). The antimicrobial effects were tested against a range of microorganisms, including Gram-negative (*Pseudomonas aeruginosa* ATCC 27853, *Klebsiella pneumoniae* ATCC 13368, *Acinetobacter baylyi* ATCC 33305, *Escherichia coli* ATCC 13846, and sodium

azide-resistant *E. coli* J53), Gram-positive (*Staphylococcus aureus* ATCC 25923 and *Staphylococcus epidermidis* ATCC 12228), and yeast species (*Candida auris* DSM 21092, *Candida parapsilosis* DSM 28722, and *Candida tropicalis* DSM 7524). Microbial suspensions were standardized to 0.5 McFarland units for bacterial strains and 1 McFarland unit for yeast strains. These suspensions were inoculated onto Mueller–Hinton agar (for bacteria) and Sabouraud agar (for yeasts). A 10 µL solution of each test sample (10 mg/mL in distilled water) was applied to the inoculated agar plates, which were then incubated at 37 °C for 24 h. Antimicrobial activity was evaluated based on the diameters of growth inhibition zones, classified into three arbitrary units (AU): 0 for no inhibition, 1 for inhibition zones $\leq$10 mm, and 2 for zones of 11–20 mm, following Corbu [23].

2.9.2. Quantitative Evaluation of the Antimicrobial Activity of the 45S5 Bioactive Glass

The evaluation of both undoped samples and samples doped with samarium was performed using the binary microdilution method in 96-well plates (ranged between 5–0.009 mg/mL) on Mueller–Hinton (MH) Broth in the case of bacterial strains and Sabouraud broth for yeast strains. Respectively, 0.5 and 1 McFarland standardized suspension was added to a final concentration of 10% in a final volume of 100 µL. After 24 h at 37 °C, the results were analyzed by determining the optical density at 620 nm using a Thermo Scientific™ Multiskan™ GO Microplate Spectrophotometer and the minimum inhibitory concentration values (MIC), based on the results analyzed in triplicate and blank subtraction.

2.9.3. Assessment of the Influence of 45S5 Bioactive Glass on Microbial Adherence

The effect of 45S5 bioactive glass on the adherence capacity of the reference bacterial and yeast strains was evaluated using an adherence inhibition assay. This assay employed sub-inhibitory concentrations of 45S5 bioactive glass samples (MIC/2 and MIC/4) and the crystal violet staining microtitration method to quantify microbial adherence. The percentage inhibition of microbial adherence (MAI%) was calculated from absorbance measurements using a previously established formula [23,24], providing a quantitative assessment of the bioactive glass's impact on the ability of microorganisms to adhere to inert substratum.

2.9.4. The Influence of 45S5 Bioactive Glass on the Soluble Virulence Factors Modulation

The ability of the reference bacterial and yeast strains to secrete soluble virulence factors (hemolysins, esculin hydrolysis, lecithinase, caseinase, and lipase) was assessed in the presence of 45S5 bioactive glass, both undoped and doped with samarium, at sub-inhibitory concentrations (MIC/2 and MIC/4). The methodology followed established protocols [25,26]. The modulation of the soluble virulence factor production was quantified by calculating the percentage inhibition of secretion, as described in prior studies [27], offering insights into the bioactive glass's potential to interfere with microbial pathogenicity.

2.9.5. Statistical Data Analysis

The data regarding antimicrobial activity, anti-adherence effects, and modulation of virulence factor production were processed using GraphPad Prism v10 (GraphPad Software, San Diego, CA, USA). Results were reported as mean values $\pm$ standard deviation (SD). A two-way analysis of variance (ANOVA) was conducted, followed by Dunnett's multiple comparisons test to account for multiple testing. A p-value < 0.05 was considered statistically significant.

3. Results and Discussion

3.1. Thermogravimetry (TG) and Differential Scanning Calorimetry (DSC) Analysis

Thermal analyses were performed on the bioactive glasses before and after the heat treatment was applied. The pristine samples contained nitrate compounds (sodium, calcium, and samarium) that had to be removed for increasing bioactivity, hence the need for a thermal treatment. The mass loss curves as a function of temperature and also DSC curves of the samples before heat treatment are presented in Figure 1. It can be observed that the mass loss takes place in four temperature ranges. In the range of 50–210 °C, the water in the bioglass composition evaporates (decomposition of crystal hydrates). In the range of 210–560 °C, the decomposition of sodium nitrate takes place with the elimination of nitrogen oxides and oxygen, and in the range of 560–700 °C, the decomposition of calcium and samarium nitrate occurs, mainly with the elimination of nitrogen oxides and oxygen. In the range 735–800 °C, a mass loss process is observed, which is assumed to be the loss generated by the decomposition of minute carbonate quantities obtained due the presence of organics in the initial composition. The shape of the curves for all four samples is similar, with a slight difference in the case of undoped 45S5 bioactive glass, where the mass loss occurs faster in the first two intervals. A slight difference appears, however, in the case of the bioglass doped with 3% samarium. This sample shows a more significant mass loss in the temperature interval 560–700 °C than the samples doped with 0.1% and 1%, which have a slower mass loss in this range. Towards the end of the experiment, the mass loss in the case of all four samples is around 50% compared to the initial mass.

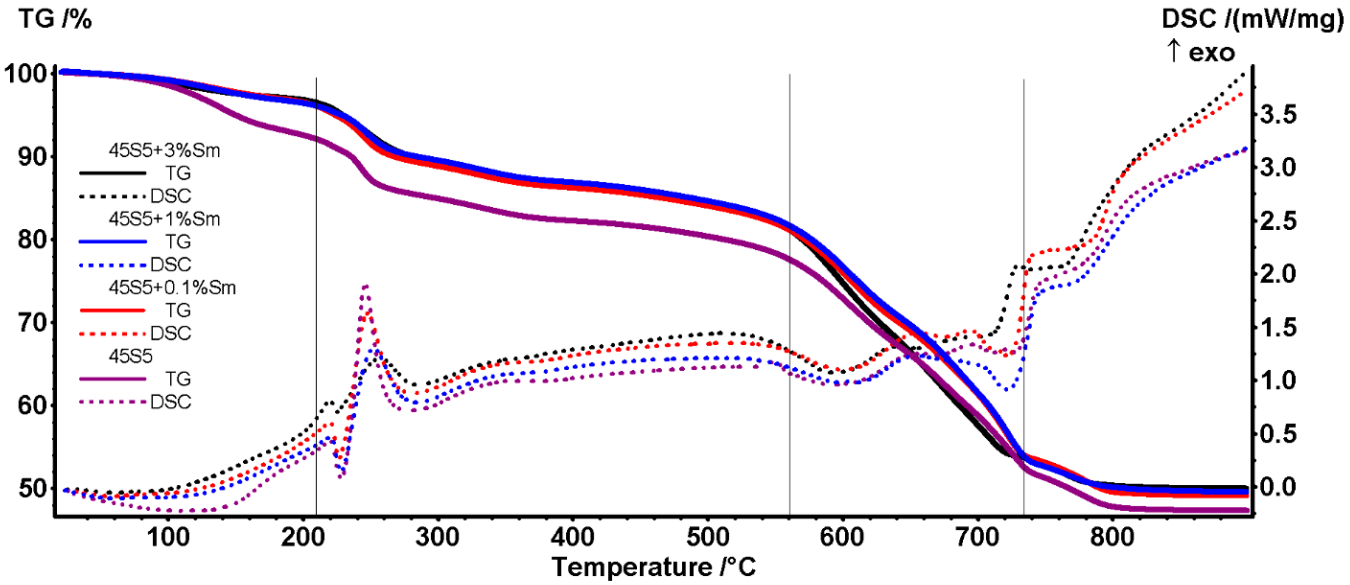

Figure 1. TG-DSC curves for raw bioactive glass (without heat treatment at 700 °C).

The glass transition of the pristine 45S5 samples was determined at 557.5 °C, in good agreement with the literature [28,29]. The samples containing Sm present a higher temperature for the glass transition, in the interval 571–576 °C. Two weak exothermic peaks are observed at ~655 °C and ~694 °C, related to oxidation processes [30]. The exothermic event from ~743 °C can be assigned to structural modifications, probably associated with the formation of crystalline phases [28]. The samarium doping has a significant impact only at a higher concentration, 3%, when the crystallization peak is observable at 730.6 °C.

Following the first thermogravimetric experiment, we found that the optimal temperature to perform the heat treatment of the bioactive glasses obtained is around 700° C. Thus, the decomposition of all nitrates is achieved and the carbonates can slowly decom-

pose during the isothermal treatment for 3 h, resulting in the bioactive glasses of the proposed composition.

The obtained samples were also subjected to thermogravimetric analysis after the heat treatment at 700 °C/3 h was performed. The mass loss and DSC curves are illustrated in Figure 2. In the case of the heat-treated samples, the mass loss was only 4%. This was due to the removal of absorbed water and carbon dioxide from the air by the bioglass after heating to 700 °C, and thus only adsorbed water is removed in this case (which is adsorbed from the air). The slopes of the curves are similar for all four samples, but it is observed that with the increase in the amount of samarium in the bioglass, the mass loss is more pronounced. This loss is most likely due to the smaller particle size of the sample with 3% Sm, as indicated by the SEM micrographs. A smaller particle size leads to a higher surface and therefore to a larger adsorption capacity of water molecules from the atmosphere.

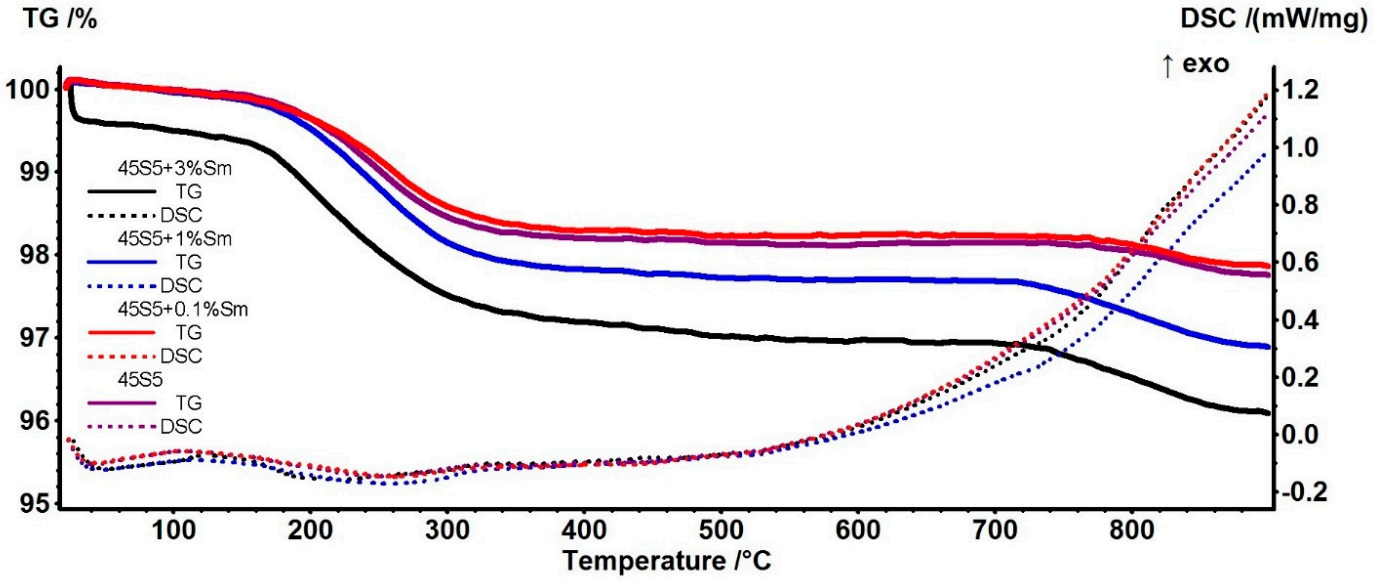

Figure 2. TG-DSC curves for bioactive glasses after the heat treatment at 700 °C/3 h.

3.2. Evaluation of Surface Morphology of Bioactive Glass Samples by SEM

The surface morphology of bioactive glasses was analyzed by SEM and is shown in Figures 3–5. In Figure 3, at a magnification of 200×, it can be seen that the powders appear as irregularly shaped granules under 500 μm in size.

In Figure 4, at a magnification of 2000×, it is observed that the bioactive glass particles represent agglomerations of smaller particles, which can be seen very clearly in Figure 5. These microparticles have a polyhedral shape, the size of which decreases with the increase in the content of Sm. In the case of the sample with +3% Sm content, the smaller particles have a size of 40–60 nm, which is in close agreement with the data reported in the literature [31]. The SEM images do not show clear evidence of porosity. Additionally, BET analysis indicates that the material has lower porosity.

From the EDS spectra, shown in Figure 6, the elemental composition of the obtained bioactive glasses can be observed. The detected X-ray lines for each element correspond to the K-series, except for Sm, which was detected using the L-series. The EDS spectra (a) and (b) of bioactive glass 45S5 and 45S5 + 0.1% Sm appear very similar, as the Sm content in sample (b) is below the detection limit of the technique. The peaks characteristic of the elements Na, O, Si, P, and Ca in the composition of bioactive glasses are observed. In the spectra (c) and (d) of the bioglass doped with a higher content of 1 and 3%

samarium, respectively, apart from the mentioned elements, the characteristic Sm peaks are also observed, which proves that the doping of bioactive glasses with samarium took place successfully.

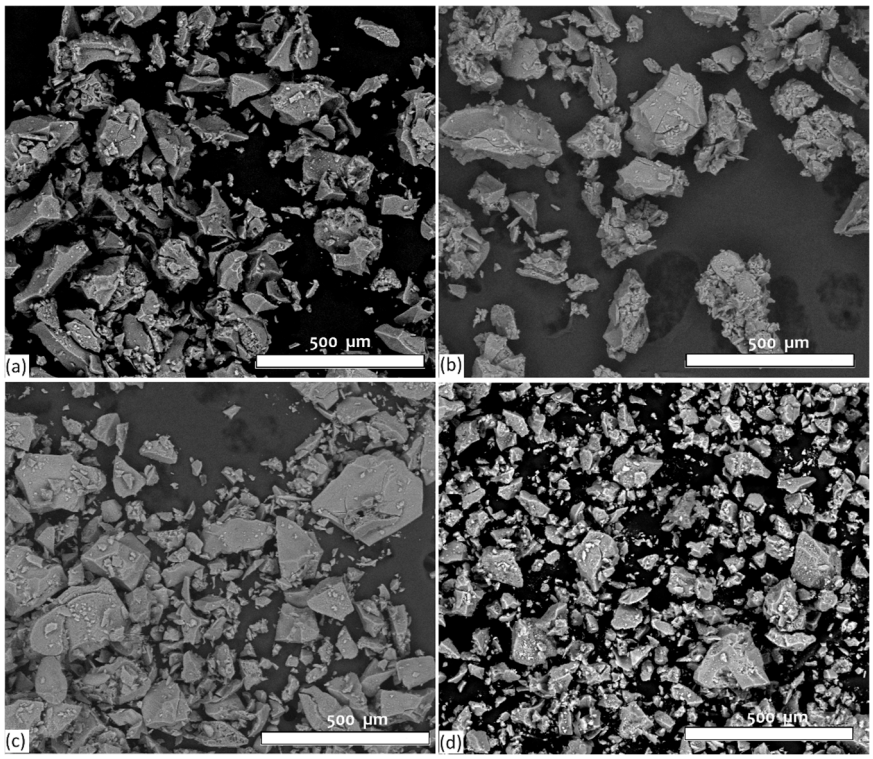

Figure 3. SEM micrographs of the bioactive glass powders at 200× magnification: (**a**) 45S5; (**b**) 45S5 + 0.1% Sm; (**c**) 45S5 + 1.0% Sm; and (**d**) 45S5 + 3.0% Sm.

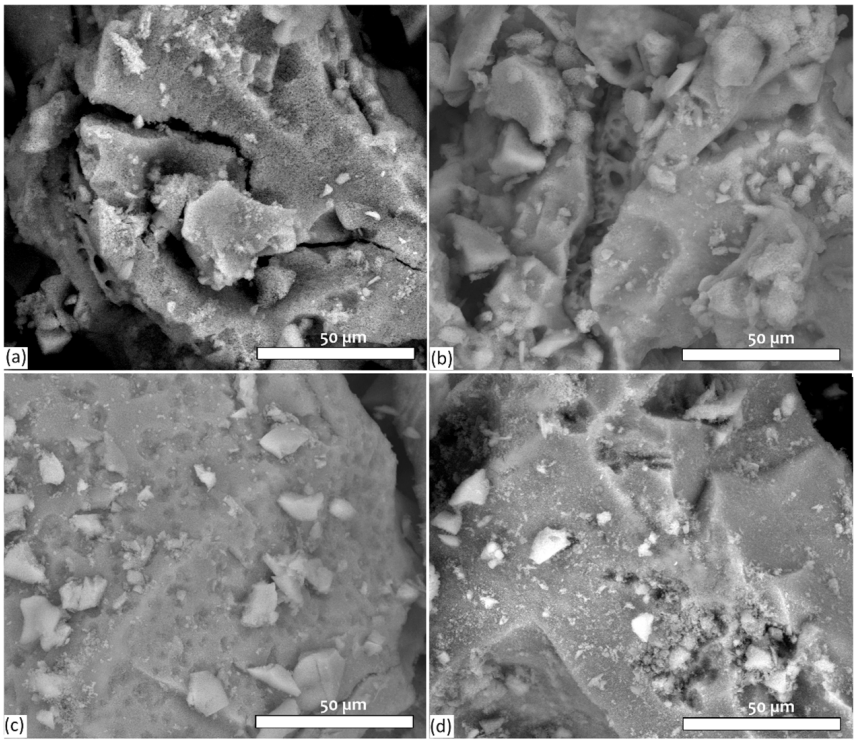

Figure 4. SEM micrographs of the bioactive glass powders at 2000× magnification: (**a**) 45S5; (**b**) 45S5 + 0.1% Sm; (**c**) 45S5 + 1.0% Sm; and (**d**) 45S5 + 3% Sm.

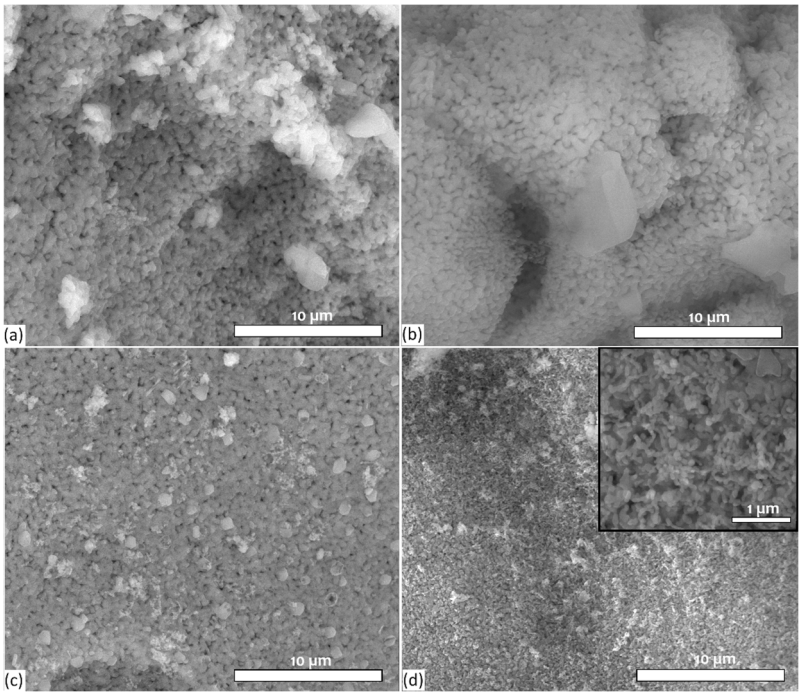

Figure 5. SEM micrographs of the bioactive glass powders at 10,000× magnification: (**a**) 45S5; (**b**) 45S5 + 0.1% Sm; (**c**) 45S5 + 1.0% Sm; and (**d**) 45S5 + 3.0% Sm.

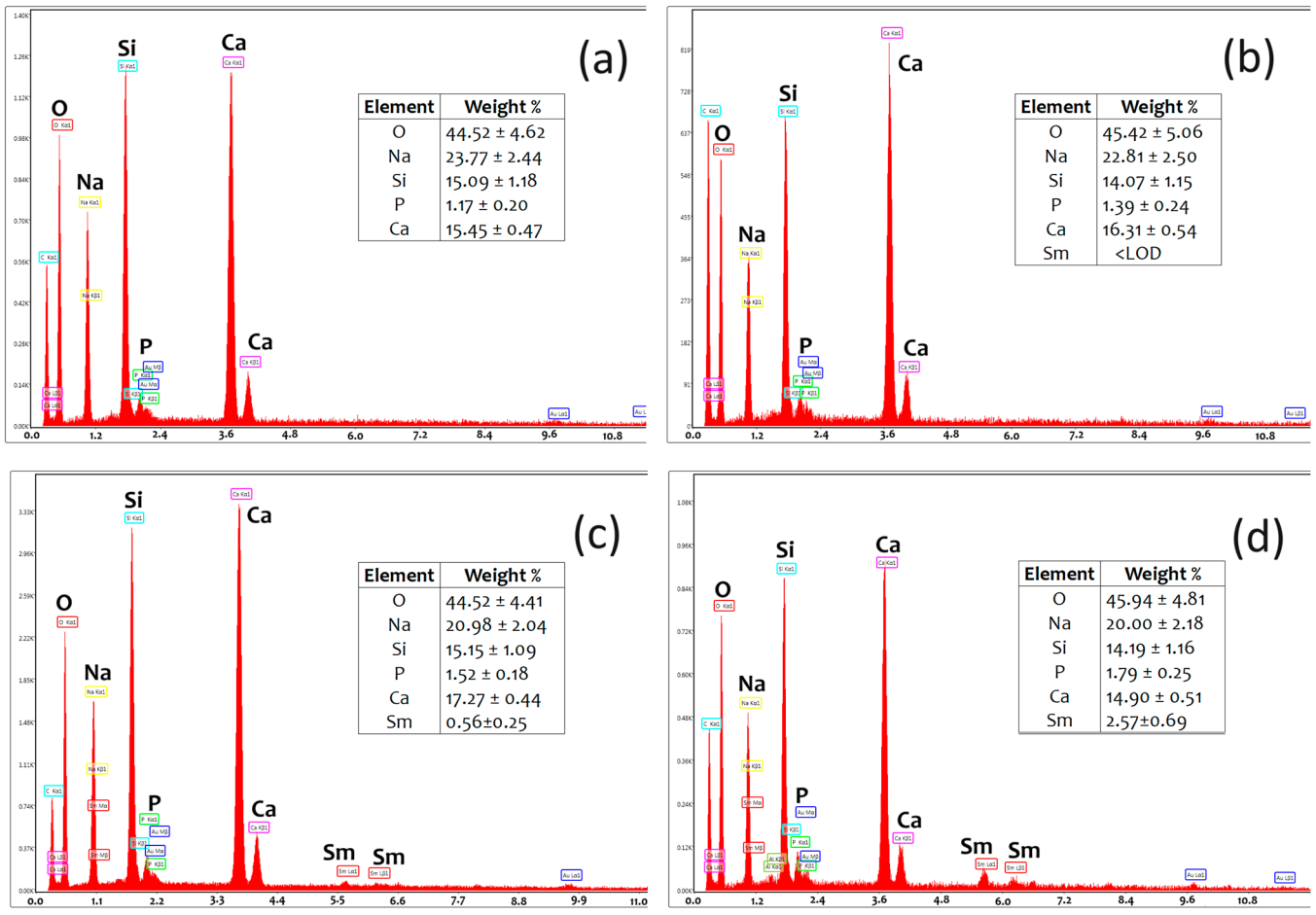

Figure 6. EDS analysis of bioactive glass (**a**) 45S5; (**b**) 45S5 + 0.1% Sm; (**c**) 45S5 + 1.0% Sm; and (**d**) 45S5 + 3% Sm.

3.3. FTIR Spectroscopy

Bioactive glass samples were analyzed by FTIR spectroscopy to monitor the presence of the characteristic peaks of bioactive glass and to observe whether nitrates were completely removed from the sample composition. With the help of this analysis, the differences that appear in the spectra of the obtained bioglass can be highlighted. Figure 7 shows the spectra obtained from the FTIR analysis.

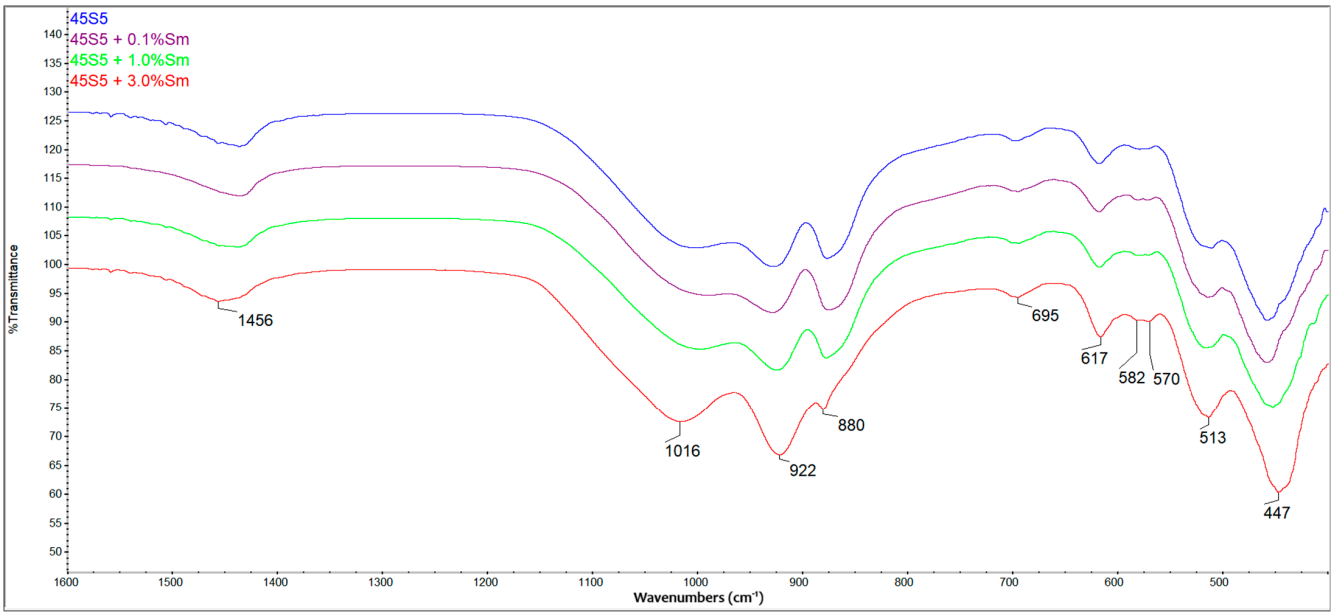

Figure 7. FTIR spectra of bioactive glass samples after the heat treatment.

The characteristic peaks of bioactive glass are observed, the shape of the curves being similar for all samples, with small differences in the shifting of the peaks, shifts that are due to the presence of samarium ions. The peaks appearing at 1436–1456 cm^{-1} signal the presence of an amount of the C-O bond from carbonate and those at 992–1016 cm^{-1} are associated with the asymmetric stretching vibration of the Si-O-Si bond. The peak at 922–930 cm^{-1} is attributed to the Si-O bond with unbound oxygen, while those at 875–880 cm^{-1} are also associated with the Si-O bond. Additionally, the peaks observed at 617 cm^{-1} and 517–510 cm^{-1} indicate the presence of silicorhenanites, representing the characteristic bending vibration of the P-O bond and the O-Si-O bond, respectively [32,33]. The peaks at 570 cm^{-1} that are less intense are due to the bending vibration of the P-O bond [34]. It can be seen from the spectra that with the increase in the samarium content, the peak at 1016 cm^{-1}, characteristic of the amorphous phase, intensifies, while the intensity of the peak at 880 cm^{-1}, associated with the crystalline phase, decreases. These data are consistent with the spectra of bioactive glass 45S5 obtained using the sol–gel method [31].

3.4. X-Ray Diffraction Analysis

Figure 8 presents the X-ray diffraction (XRD) patterns of the synthesized pristine 45S5 bioglass and the samples doped with 0.1%, 1%, and 3% samarium (Sm). Regardless of the nominal composition, the patterns indicate a mixture of combeite ($Na_{2.915}Ca_{1.543}Si_3O_9$—COD # 96-900-7712 [35]) and devitrite ($Na_2Ca_3Si_6O_{16}$ [36]) as crystalline phases and the glassy phase. At low Sm addition levels of 0.1% and 1%, the devitrite content decreases from 3.8% to approximately 1.3–1.4%. However, increasing the Sm addition to 3% results in a rise in devitrite content to 4.5% (see Table 3). The non-monotonic trend in devitrite content suggests a competing effect of samarium ions: inhibition of devitrite nucleation at low concentrations due to structural disruption versus enhanced

crystallization at higher concentrations due to increased phase separation or nucleation sites. An interesting aspect is the crystallinity degree of the samples, around 19%, which is lower than the values reported in the literature [31]. This can be explained by a phenomenon where the crystalline phase is shelled within a more amorphous phase, thereby reducing the measured crystallinity.

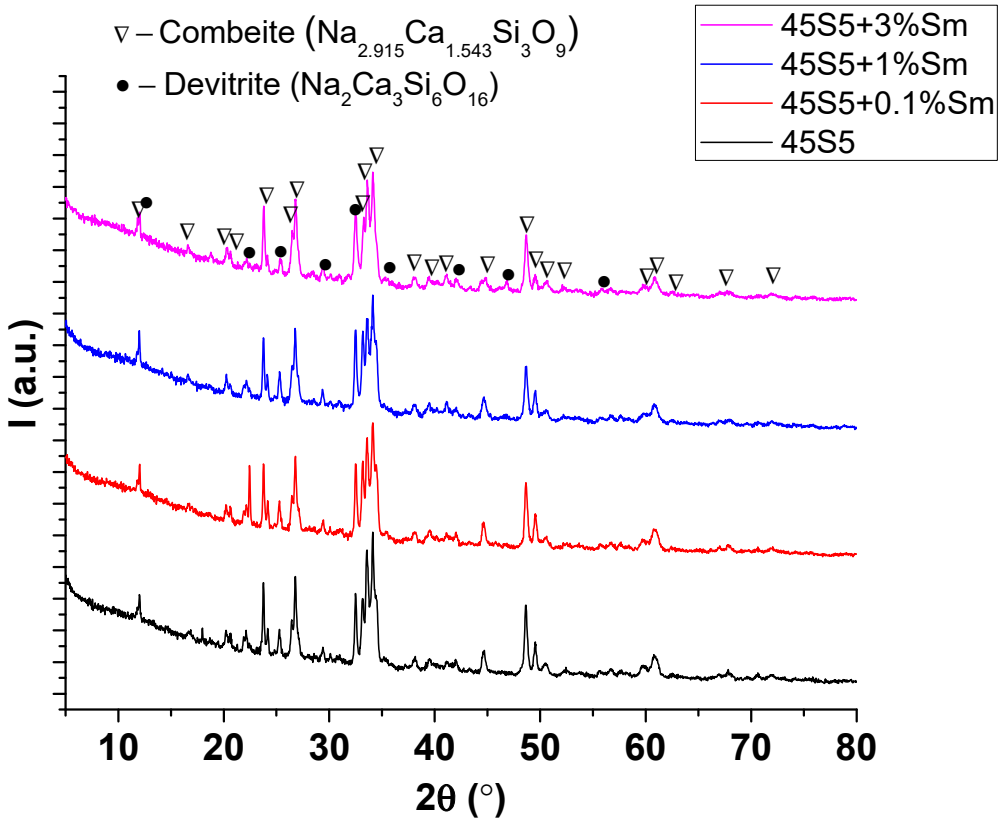

Figure 8. X-ray diffraction patterns of 45S5 bioglass with varying samarium additions.

Table 3. Crystalline phase composition of 45S5 bioglass with varying samarium additions.

Sample	Combeite	Devitrite
45S5	96.2%	3.8%
45S5 + 0.1% Sm	98.7%	1.3%
45S5 + 1% Sm	98.6%	1.4%
45S5 + 3% Sm	94.5%	4.5%
45S5 + 3% Sm after 21 days in SBF	97.5%	1.3%

The incorporation of the samarium in the crystalline phases of the 45S5, 45S5 + 0.1% Sm, 45S5 + 1% Sm, and 45S5 + 3% Sm samples was studied by analyzing peak positions and unit cell parameters obtained from Rietveld refinements. Thus, the variation of devitrite phase peak positions to higher 2θ values accompanied by a decrease its unit cell volume (Table 4) with the increasing content of samarium show the incorporation of Sm^{3+} in the devitrite phase. Considering the ionic radius of Sm^{3+} (1.24 Å) and the ionic radius of Na^+ (1.39 Å) and Ca^{2+} (1.34 Å) ions, doping most probably takes place by a partial replacement of the Na^+/Ca^{2+} ions with Sm^{3+}, which explains the decrease in the unit cell volume when increasing the samarium addition.

Table 4. Unit cell parameters of 45S5 bioglass crystalline phases with varying samarium additions.

	45S5		**45S5 + 0.1% Sm**		**45S5 + 1% Sm**		**45S5 + 3% Sm**	
	Combeite	**Devitrite**	**Combeite**	**Devitrite**	**Combeite**	**Devitrite**	**Combeite**	**Devitrite**
a (Å)	10.497	10.203	10.498	10.111	10.492	10.102	10.497	10.131
b (Å)	10.497	10.699	10.498	10.691	10.492	10.627	10.497	10.584
c (Å)	13.179	7.174	13.179	7.171	13.170	7.102	13.164	7.043
α (°)	90	110.86	90	110.8	90	109.90	90	109.13
B (°)	90	97.78	90	98.2	90	98.10	90	98.13
ɣ (°)	120	78.10	120	78.01	120	78.16	120	78.18
V/10^6 (pm^3)	1257.737	714.3854	1257.862	706.8171	1255.539	699.5542	1256.095	696.1263

After the immersion of 45S5 bioglass doped with 3% Sm in SBF for 21 days, the XRD pattern (Figure 9) highlights the formation of a 1.2% hydroxyapatite phase (COD # 96-900-2217 [37] with a low crystallinity specific for the such bioactivity studies in SBF), while the content of devitrite decreases from 4.5% to 1.3% and the combeite phase increases from 94.5% to 97.5% (Table 5). Notably, the intensity of the peaks decreases after immersion in SBF, which corresponds to a reduction in crystallinity from 19.36% to 11.68%, which is normal because the apatite phase deposition (coating) is a wet precipitation process. Even if the content of the hydroxyapatite is only 1.2%, this value is significant because the crystallinity of the formed HA is low. In fact, the most important conclusion is that these samples are bioactive, the kinetics being important but not crucial.

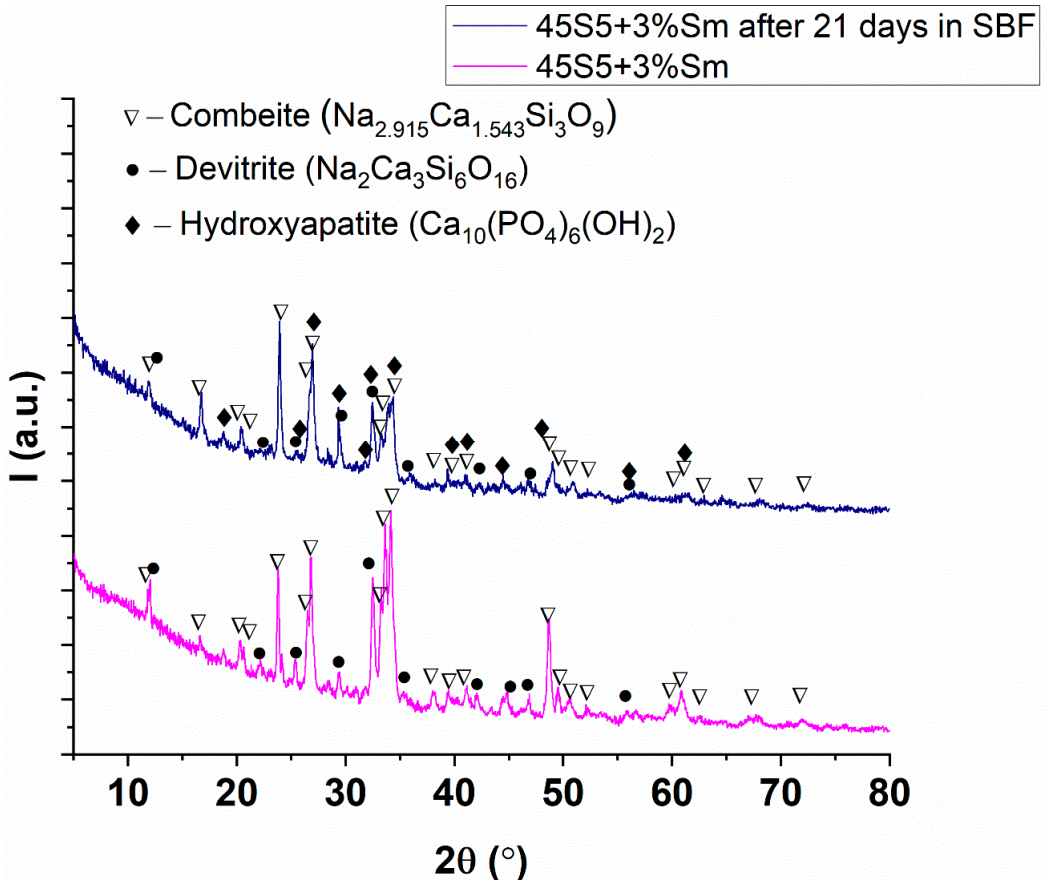

Figure 9. X-ray diffraction patterns of 45S5 bioglass doped with 3% Sm before and after 21 days of immersion in SBF.

Table 5. Phase composition of 45S5 bioglass doped with 3% Sm before and after 21 days of immersion in SBF.

Sample	Combeite	Devitrite	Hydroxyapatite
45S5 + 3% Sm	94.5%	4.5%	-
45S5 + 3% Sm after 21 days in SBF	97.5%	1.3%	1.2%

3.5. Density Determination and Textural Characteristics of the Bioactive Glasses

The results of density determinations of the bioactive glasses synthesized in this work are graphically represented in Figure 10. It can be observed that the density of the glasses increases with the increase in the amount of samarium. This density increase can be attributed to the substitution of lighter silicon ions with heavier samarium ions, a phenomenon also reported by the authors of reference [38].

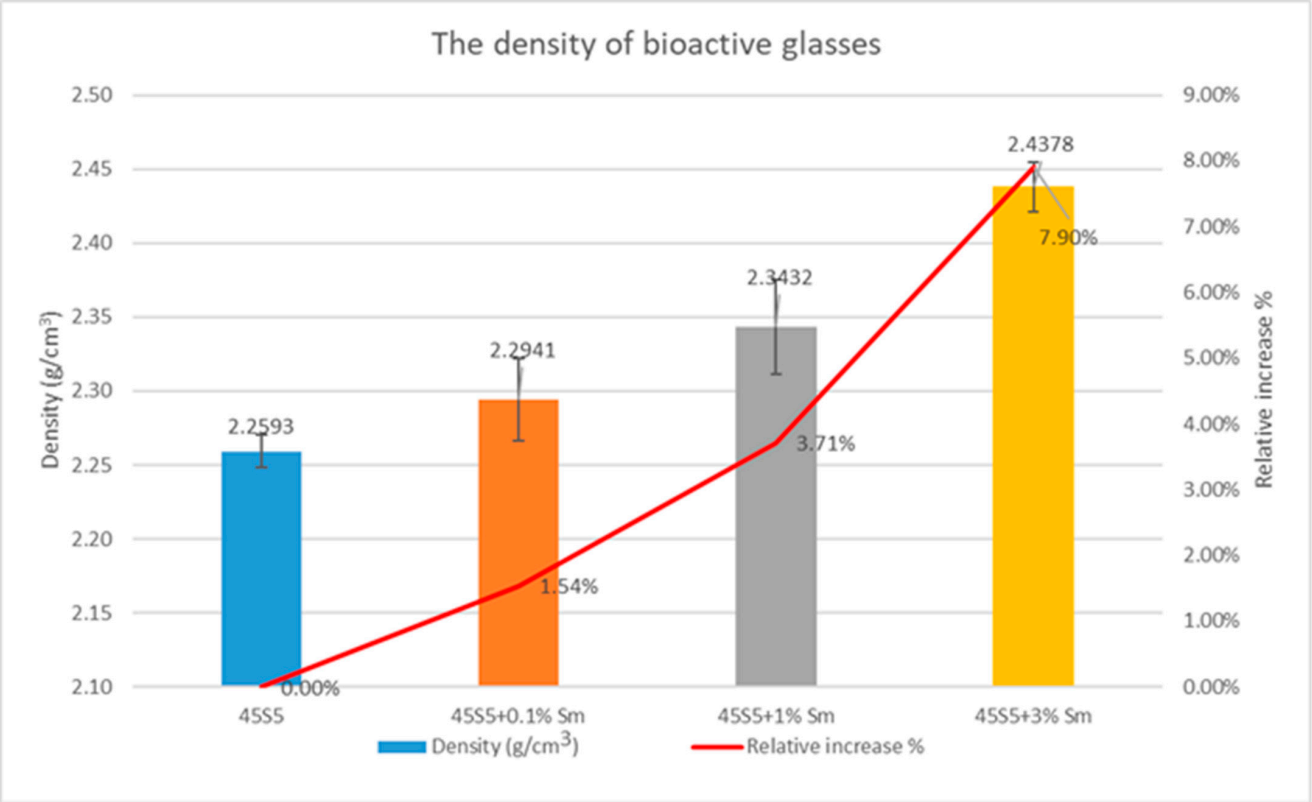

Figure 10. Density values of simple and samarium-doped 45S5 bioactive glass.

The textural characteristics of bioactive glasses, such as specific surface area, pore volume, and pore diameter, are presented in Table 6. The results show that the specific surface area of the samples ranges between 1.37 and 7.4 m^2/g, while the pore volume is very low, bellow the quantification level, and thus we can just conclude that the bioactive glasses are not porous. The average pore diameter ranges from 3.5 to 3.88 nm. These values suggest a low porosity, typical of non-porous bioactive glasses. Although mesoporous glasses have the ability to form apatite in SBF in vitro and exhibit higher cytocompatibility compared to non-porous glasses [39], the bioglasses obtained in this work demonstrate a good capacity to form apatite while maintaining good biocompatibility, as will be discussed in the following sections.

Table 6. N_2-BET surface area of bioactive glass.

Sample	Surface Area (m^2/g)	Pore Volume (cm^3/g)	Pore Diameter (nm)
45S5	2.690	<LQ	3.525
45S5 + 0.1% Sm	7.387	<LQ	3.883
45S5 + 1.0% Sm	1.370	<LQ	3.863
45S5 + 3.0% Sm	2.060	<LQ	3.880

LQ: Limit of Quantification.

3.6. Bioactivity Evaluation Using FTIR

The bioactivity of the samples obtained was evaluated by immersing them in SBF and tracking the change in the composition of the powders after different periods of time. The composition of the powders was analyzed by FTIR spectroscopy. Figure 11 shows the FTIR spectra of bioactive glass samples doped with 3% samarium before and after immersion in SBF at 36.5 °C ± 0.5 °C and a pH value of 7.4 (conditions similar to those present in the human body).

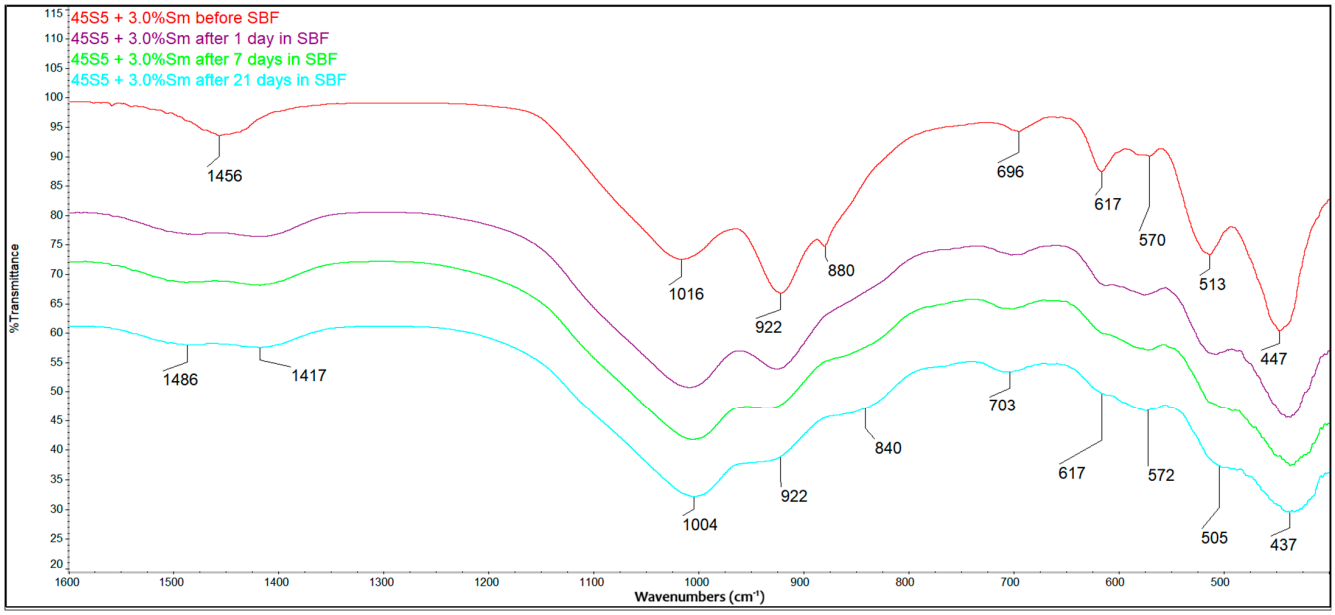

Figure 11. FTIR spectra of the bioactive glass powder doped with 3% samarium, before and after immersion in SBF.

From the spectra obtained, the formation of HCA can be observed from the first day of immersion in SBF. As the immersion time in SBF progresses, the intensity of certain characteristic peaks decreases, and some of them undergo a shift in their position. The peak that appears at 1456 cm^{-1}, characteristic of the C-O bond in carbonates, shifts into two peaks that appear at 1480 and 1417 cm^{-1}, associated with the stretching vibration of the C-O bonds in HCA which are going to be formed during the bioactivity assessment. The peak at 570 cm^{-1}, which corresponds to the bending vibration of the P-O bond, has been present and remains observable. The peak at 1005 cm^{-1} associated with the asymmetric Si-O-Si stretching vibration remains present even after 21 days of immersion in SBF. On the other hand, the intensity of the 922 and 880 cm^{-1} peaks attributed to the Si-O bond with the unbound oxygen decreases with time. These spectral transformations demonstrate the formation of hydroxycarbonated apatite (especially based on the intensifying of the peak from 1004 cm^{-1}) on the bioglass surface during the immersion in SBF.

3.7. Determination of the pH Variation and the Ionic Strength of SBF Solution

The variation of pH and ionic strength of the SBF used was monitored during the bioactivity testing of the samples in order to determine if any ions were released into the solution. The obtained results are presented in Figures 12 and 13. It is observed that the pH of the SBF solution increases over time, especially in the first days. This can be explained by the fact that the release of cations from the bioactive glass network takes place, and they are replaced by hydronium ions. There is also a dependence between the pH of the solution and the amount of dopant ion. The higher the concentration of samarium, the greater the increase in pH and conductivity. However, this increase is not significant, in the case of samples with 1% and 3% samarium, respectively, the values being extremely close. A higher pH in the solution can be an advantage for the bioactive glass, as it suggests a higher dissolution rate, which could facilitate the formation of hydroxyapatite on the surface of the material. This is an important indicator of bioactivity, as hydroxyapatite formation is crucial for bone tissue bonding and integration. Furthermore, an elevated pH may improve the material's affinity for bone tissue, as more alkaline conditions are known to promote the formation of hydroxyapatite, essential for the integration of implants into the bone [40].

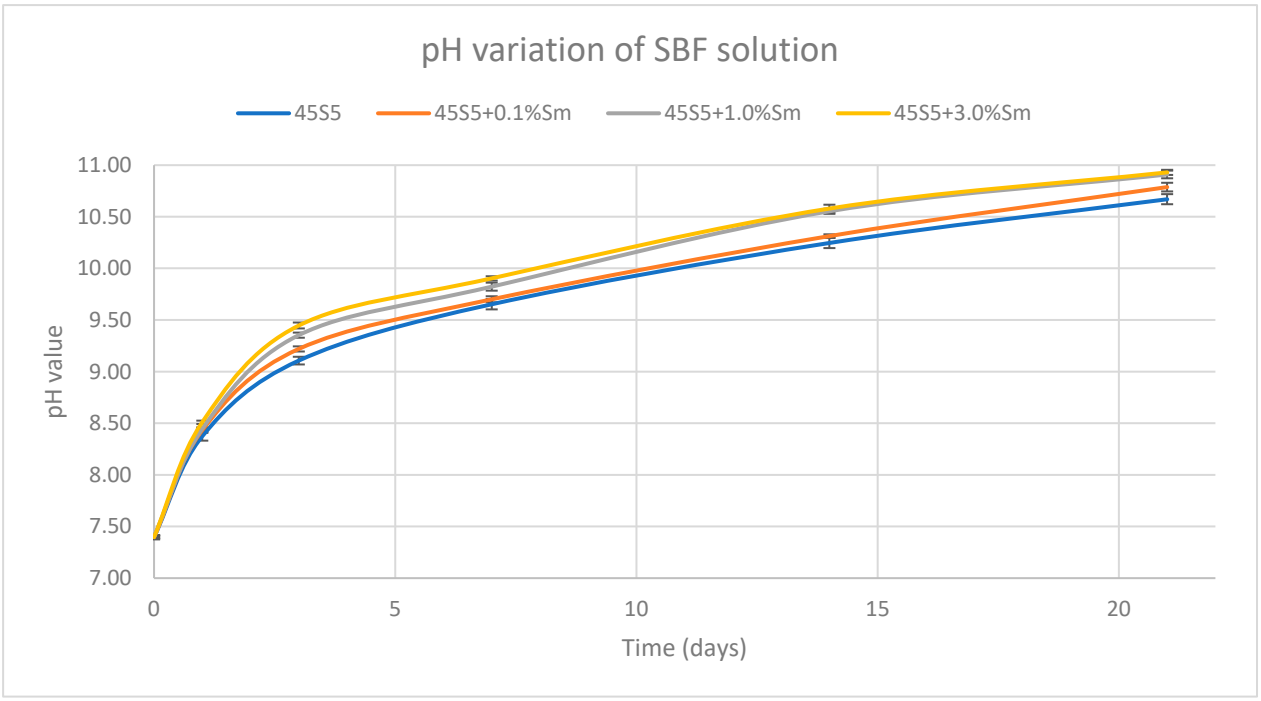

Figure 12. pH variations of the SBF solution during the evaluation of bioactivity of the bioactive glass doped with samarium.

Additionally, the increase in pH may have antimicrobial effects, as certain bacteria and biofilms are sensitive to changes in pH. In this context, samarium doping could provide an added benefit in preventing infections, offering a dual advantage of both enhanced bioactivity and antimicrobial properties [41].

In Figure 13, the variation of the ionic strength of the SBF solutions is represented during the in vitro assessments. A rapid increase in conductance is observed in the first 3 days, which continues in the following days but is significantly more slowly. From the graphic representation, a dependence of the conductance variation on the amount of dopant ion can be observed. The greater the amount of samarium in the sample, the greater the amount of ions released into the SBF solution. The slightly higher conductivity values

observed in the samples with higher samarium concentrations suggest a greater release of ions from the doped glass into the SBF solution. This phenomenon may indicate a slightly more pronounced dissolution of the glass network and a more intense ion exchange, factors that could contribute to enhanced bioactivity.

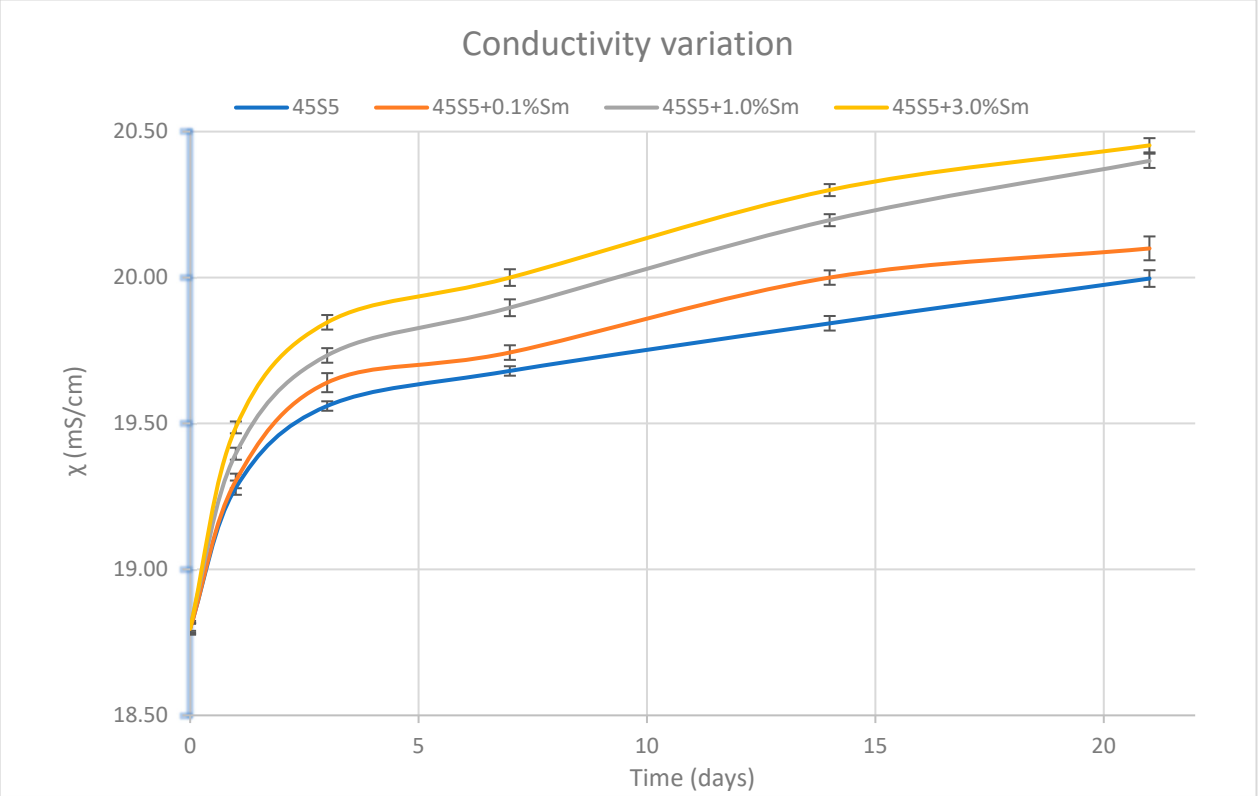

Figure 13. The variation of the ionic strength of the SBF solution during the evaluation of the bioactivity of bioactive glasses doped with samarium.

Considering the changes of the pH and conductivity, it can conclude that the three Sm-doped bioactive glasses are slightly more active.

3.8. Mass Loss Determination

To determine if the solubility of the bioactive glass is influenced by the amount of doping agent used, the mass loss of the samples was determined. For this, after performing the in vitro test, the bioactive glass samples were filtered, dried at 105 °C/1 h, and then weighed. After comparing the initial and final masses, we concluded that during the test, a partial dissolution of the bioactive glass takes place, which leads to a loss of mass up to approx. 13% after 21 days of immersion (Figure 14). The greatest loss of mass occurs on the first day of immersion. The bioglass undergoes transformations immediately after immersion in SBF, the soluble ions being released into the solution very quickly. After the first day of immersion, the bioglass continues to undergo transformations, but much slower, which indicates a rapid, immediate response at the contact with the biological environment and a very good bioactivity. A slightly higher loss is also observed in bioactive glasses doped with a larger amount of samarium, which correlates with the data presented on the variation of pH and ionic strength. It is worth mentioning that the overall measured difference is a complex function which keeps in mind solubilization and deposition processes. As an overall conclusion, the higher the samarium content is, the higher the activity in SBF is.

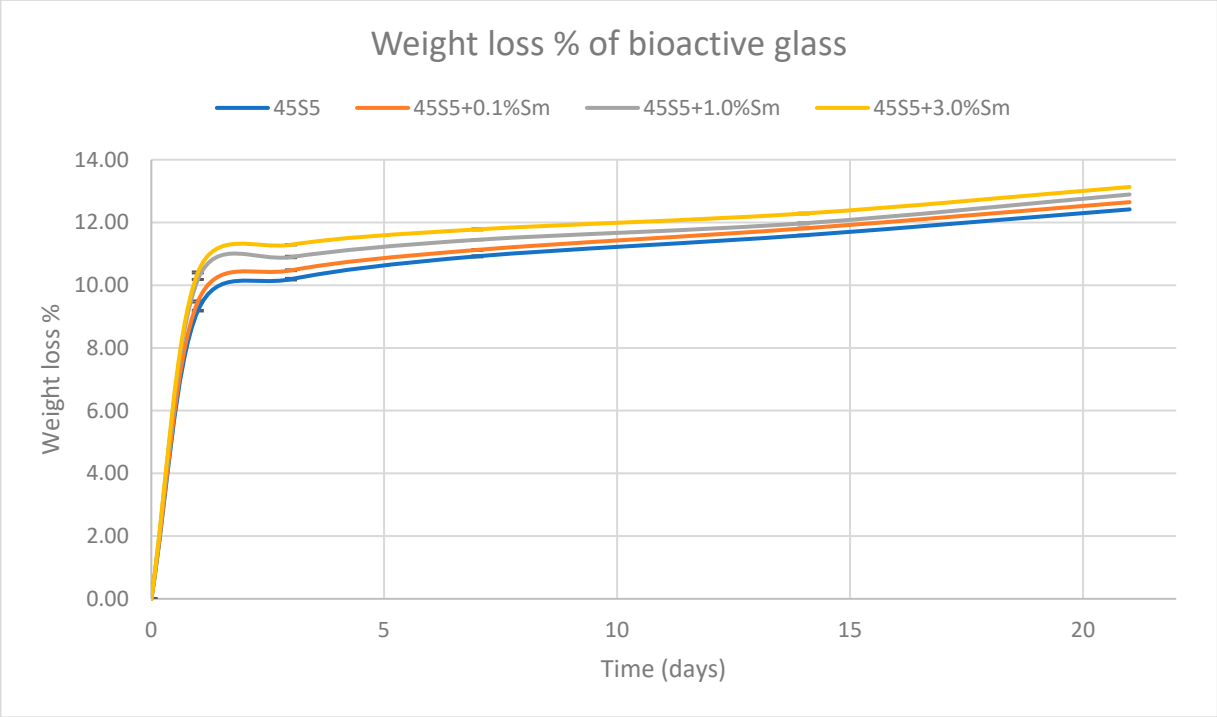

Figure 14. Mass loss of the bioactive glasses during in vitro testing.

3.9. Biocompatibility Test Results

First of all, the optimization of the working concentration was performed analyzing several concentrations (from 1 to 50 mg/mL) of the composition with the highest concentration of samarium, due to the biophysical-chemical properties of samarium. Live/Dead staining was used to highlight the ratio between live and dead cells exposed to different concentrations of 45S5 + 3% Sm-conditioned media after 24 h of incubation in standard conditions (Figure 15). The results revealed high cell viability in contact with 1 mg/mL, 5 mg/mL, 10 mg/mL, and 20 mg/mL of 45S5 + 3% Sm, as compared with the same concentration of simple 45S5 bioactive glass. Moreover, higher concentrations (40 mg/mL and 50 mg/mL) of bioactive glasses determined a decrease in cell viability both in contact with 45S5 and 45S5 + 3% Sm bioactive glasses. Based on Live/Dead results, a working concentration of 20 mg/mL was established for carrying out the biological assays.

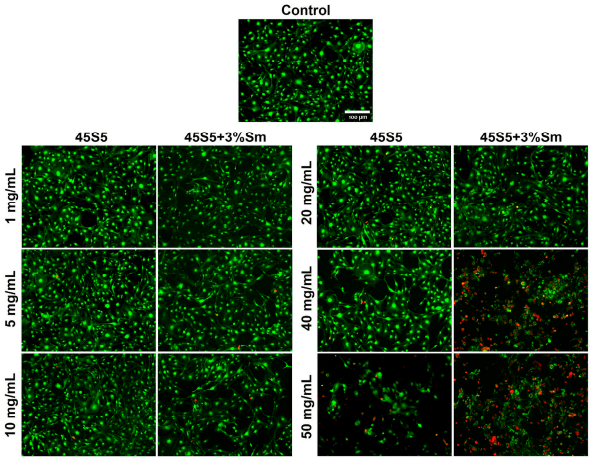

Figure 15. Qualitative Live/Dead staining revealing live cells (green fluorescence) and dead cell nuclei (red fluorescence) of MC3T3-E1 cells in contact with different concentrations of 45S5 + 3% Sm-conditioned media after 24 h of incubation in standard conditions. Scale bar 100 µm.

The LDH assay indicated an overall low level of LDH released by the MC3T3-E1 cells in contact with the enriched 45S5 bioactive glasses (Figure 16b). After 24 h of incubation in standard conditions, no significant differences were registered in terms of cytotoxicity between the control, 45S5, and Sm-enriched 45S5 bioactive glasses. After 48 h of incubation, similar cytotoxicity levels were observed for 45S5 and Sm-enriched 45S5 bioactive glasses, although a slight increase was registered in contact with 20 mg/mL of 45S5 + 3% Sm, compared to untreated cells. Therefore, the 45S5 bioactive glasses can be validated as biocompatible and used in bone-related applications.

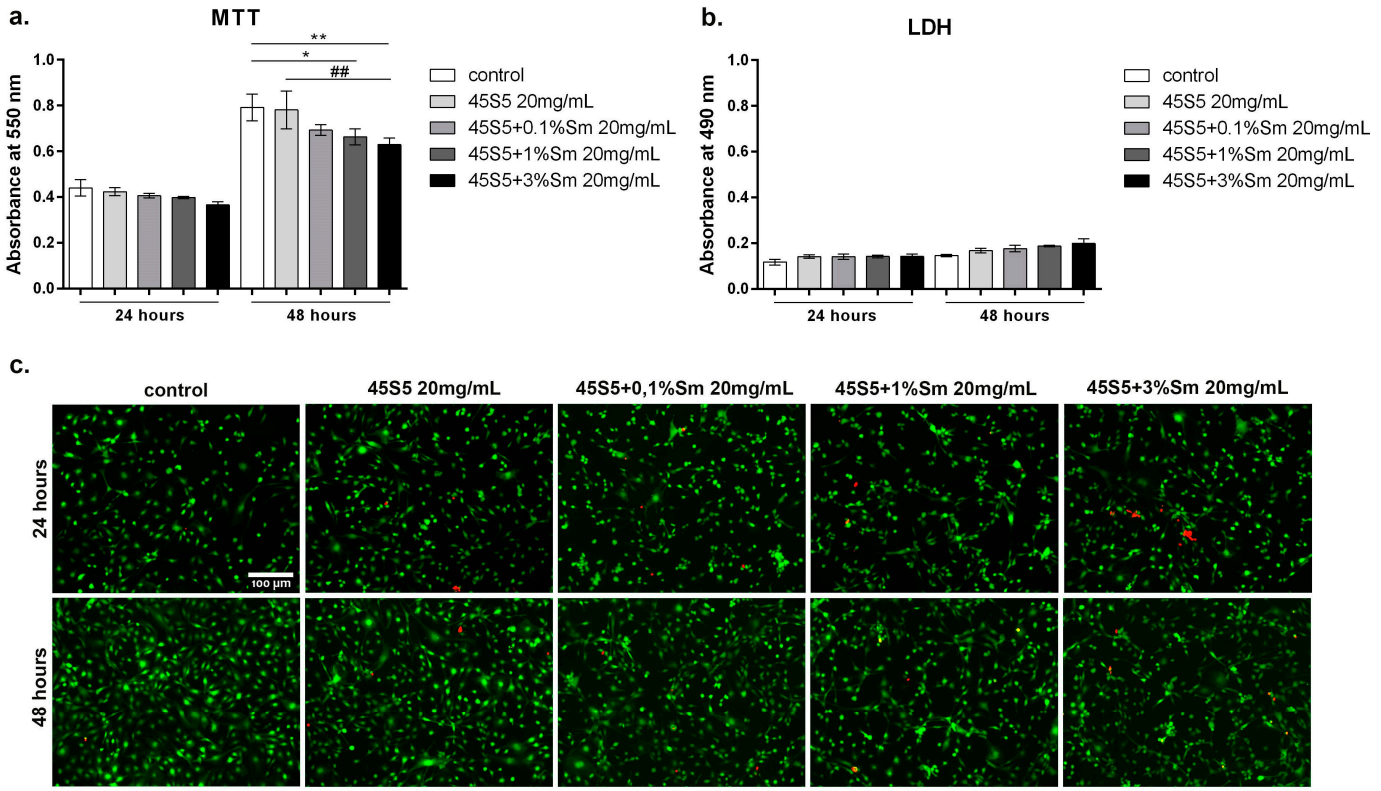

Figure 16. (**a**) Cell viability evaluation by MTT assay at 24 and 48 h after addition of 45S5-conditioned media. Statistical significance: * $p < 0.05$, ** $p < 0.01$, ## $p < 0.01$. (**b**) 45S5 bioactive glasses' cytotoxicity evaluation, as revealed by LDH assay after 24 and 48 h of incubation in standard conditions. (**c**) Qualitative Live/Dead staining revealing live cells (green fluorescence) and dead cell nuclei (red fluorescence) of MC3T3-E1 cells in contact with 45S5, 45S5 + 0.1% Sm, 45S5 + 1% Sm, and 45S5 + 3% Sm-conditioned media after 24 and 48 h of incubation in standard conditions. Scale bar 100 µm.

The Live/Dead fluorescent staining allowed the qualitative evaluation of cell distribution and viability in contact with enriched 45S5 bioactive glasses and the results were in accordance with the quantitative results obtained from MTT and LDH assays (Figure 16c). After 24 h of incubation in standard conditions, the results indicated that 20 mg/mL of 45S5 bioactive glasses supported cell viability, suggesting no negative impact on cell behavior. However, small amounts of dead cells can be observed after contact with 20 mg/mL of 45S5 + 3% Sm, compared with the control. After 48 h of incubation, a high cell density and small amount of dead cell nuclei were observed in contact with Sm-enriched 45S5 bioactive glasses, although no significant differences were noticed between compositions.

3.10. Antimicrobial and Anti-Adherence Activity and the Influence of Bioactive Glass 45S5 Doped with Samarium Against Virulence Factors' Production

The 45S5 bioactive glass doped with samarium was inefficient at combating the development of Gram-positive, Gram-negative, and *Candida* strains investigated by qualitative assays.

3.10.1. Quantitative Evaluation of the Antimicrobial Activity of the 45S5 Bioactive Glass Doped with Samarium Against Bacterial and Yeast Strains

The 45S5 bioactive glass doped with samarium showed limited antibacterial activity against most tested bacterial strains, with minimum inhibitory concentrations (MIC) ranging from 1.25 to 5 mg/mL. Nica et al., in 2021, demonstrated no antimicrobial activity of hydroxyapatite nanoparticles doped with samarium against Gram-positive bacteria (*S. aureus* and *Enterococcus faecalis*), Gram-negative bacteria (*E. coli* and *P. aeruginosa*), and yeast strains (*Candida albicans*) [42]. In our obtained results, the highest antibacterial effectiveness was observed for 45S5 + 1% Sm and 45S5 + 3% Sm against *A. baylyi* ATCC 33305 strain (MIC = 1.25 mg/mL), followed by 45S5 + 1% Sm against *S. epidermidis* ATCC 12228 (MIC = 2.5 mg/mL) (Figure 17). Lavric et al., in 2023, demonstrated the antimicrobial activity of standard bioglass doped with silver and samarium against Gram-negative bacteria, highlighting its potential application in bone grafts and implants [15]. Similarly, Araujo et al. in 2021 demonstrated the antibacterial activity of 45S5 bioglass doped with alumina and strontium oxide against *E. coli* strains through qualitative assays [43]. In another study, Hammami et al. (2023) demonstrated that incorporating CuO into 45S5 Bioglass revealed antibacterial properties against *E. coli*, methicillin-resistant *S. aureus* (MRSA), and *Streptococcus mutans* reference strains [44]. The findings highlighted its potential to prevent bacterial infections, promote osseointegration, and enhance the long-term success of implants. Furthermore, Zhang et al. (2024) developed composite scaffolds integrating polycaprolactone (PCL) with 45S5 bioglass, demonstrating enhanced antibacterial properties, as evidenced by the formation of inhibition zones against *E. coli* and *S. aureus* strains [45]. The addition of 45S5 bioglass significantly improved the composite's antibacterial efficacy while also enhancing its surface hydrophobicity, mechanical rigidity, and overall biocompatibility, making it a promising material for biomedical applications.

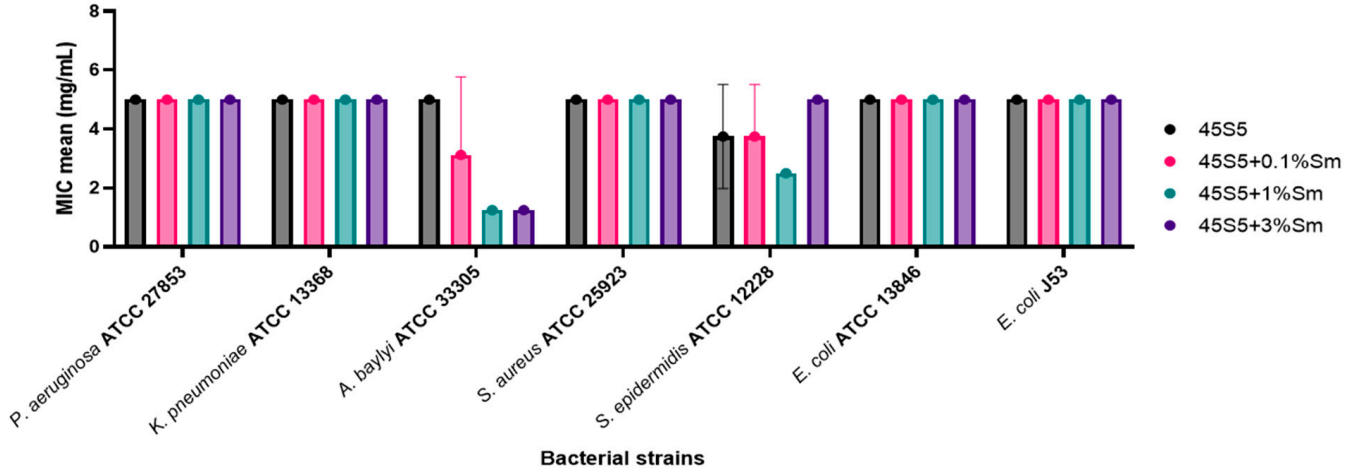

Figure 17. Graphical representation of the MIC values of 45S5 bioactive glass doped with samarium against bacterial strains.

The reported MIC values against *Candida* spp. strains are 5 mg/mL for all of the examined samples, except for 45S5 + 3% Sm which showed the best antimicrobial activity

against the three tested strains: *C. parapsilosis* DSM 28722 (CMI = 0.313 mg/mL), *C. auris* DSM 21092 (CMI = 2.5 mg/mL), and *C. tropicalis* DSM 7524 (CMI = 3.75 mg/mL) (Figure 18).

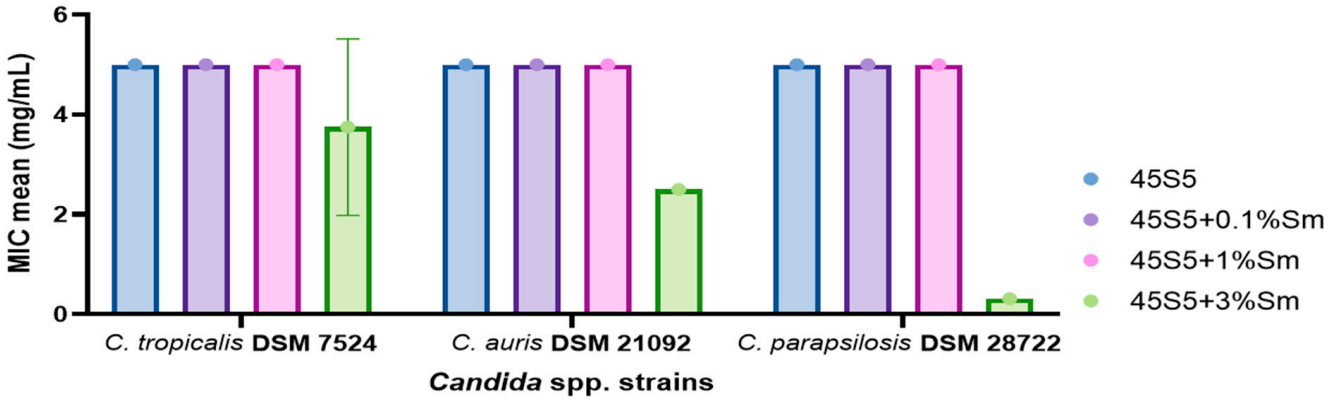

Figure 18. Graphical representation of the MIC values of 45S5 bioactive glass doped with samarium against *Candida* spp. strains.

3.10.2. The Influence of the 45S5 Bioactive Glass Doped with Samarium on the Microbial Adherence Capacity to the Inert Substratum

The impact of the bioactive glass on the adherence capacity of bacterial strains to the inert substratum highlighted that *K. pneumoniae* ATCC 13368 strain did not significantly reduce the adherence capacity to the inert substratum; moreover, the adherence was stimulated, most probably due to the fact that its presence exhibited cellular stress, which might influence the bacterial cells to form stress-resistant associations [46]. The highest reduction of the adherence capacity was observed in the case of *S. aureus* ATCC 25923 treated with all tested samples, with the percentage of adherence inhibition capacity ranging from 21–61%. The 45S5 + 3% Sm MIC/2 significantly reduced the adherence capacity of the tested *S. epidermidis* ATCC 12228 strain to the inert substratum, with the percentage values being below 10% (Figure 19). Previously, the superior antibacterial and anti-biofilm activity of 45S5 bioglass compared to S53P4 bioglass was demonstrated against MRSA and *P. aeruginosa* PAO1 strains [47]. In another study, the anti-biofilm activity of hydroxyapatite nanoparticles doped with Samarium was demonstrated against *S. aureus*, *E. faecalis*, *E. coli*, and *C. albicans* reference strains, suggesting their potential as promising candidates for novel anti-biofilm agents [42].

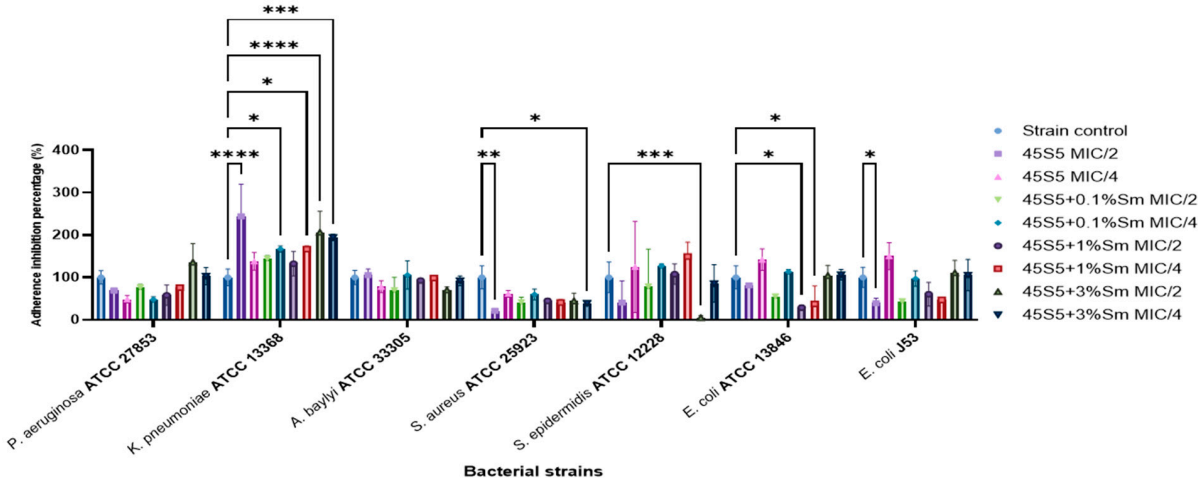

Figure 19. Graphic representation of the bacterial adherence capacity to the inert substratum (* $p < 0.05$, ** $p < 0.01$; *** $p < 0.001$, **** $p < 0.0001$).

None of the 45S5 samples and the doped variants significantly increased the adherence inhibition for *C. tropicalis* DSM 7524, with percentages remaining around or slightly higher compared to the control. On the other hand, after being exposed to 45S5 bioactive glass, both the *C. auris* DSM 21092 and *C. parapsilosis* DSM 28722 strains demonstrated significant increases in the adherence capacity, the results showing that the percentage was noticeably higher than the control. However, 45S5 + 3% Sm showed a reduction of the adherence capacity for the *C. parapsilosis* DSM 28722 strain (Figure 20).

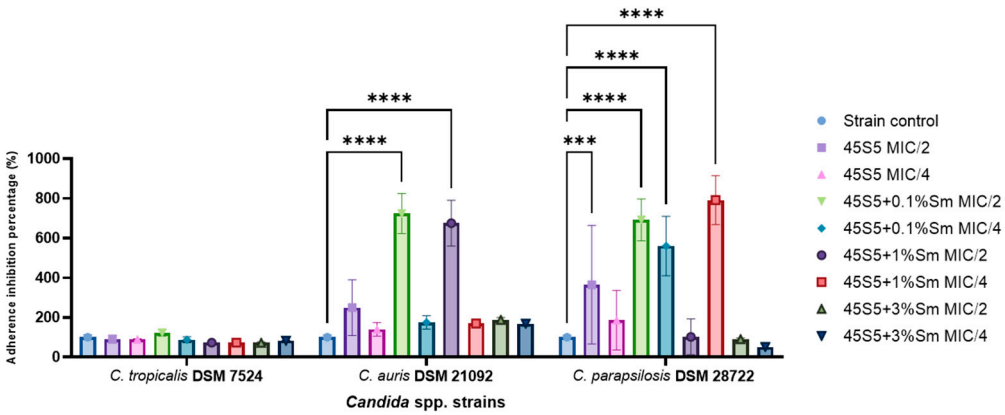

Figure 20. Graphic representation of the microbial adherence capacity to the inert substratum (*** $p < 0.001$, **** $p < 0.0001$).

3.10.3. The Influence of 45S5 Bioactive Glass Doped with Samarium on the Soluble Virulence Factors Modulation

The results of the effect of 45S5 bioactive glass, with or without samarium doping, on hemolysin production were shown across three bacterial strains: *P. aeruginosa* ATCC 27853, *S. aureus* ATCC 25923, and *S. epidermidis* ATCC 12228. The hemolysin production capacity was completely reduced (0%) in the case of the *S. epidermidis* ATCC 12228 strain. Meanwhile, it was observed that a slight inhibition in the case of *S. aureus* ATCC 25923 treated with 45S5 + 3% Sm both MIC/2 and MIC/4, with percentages ranging from 58.33%–75% (Figure 21).

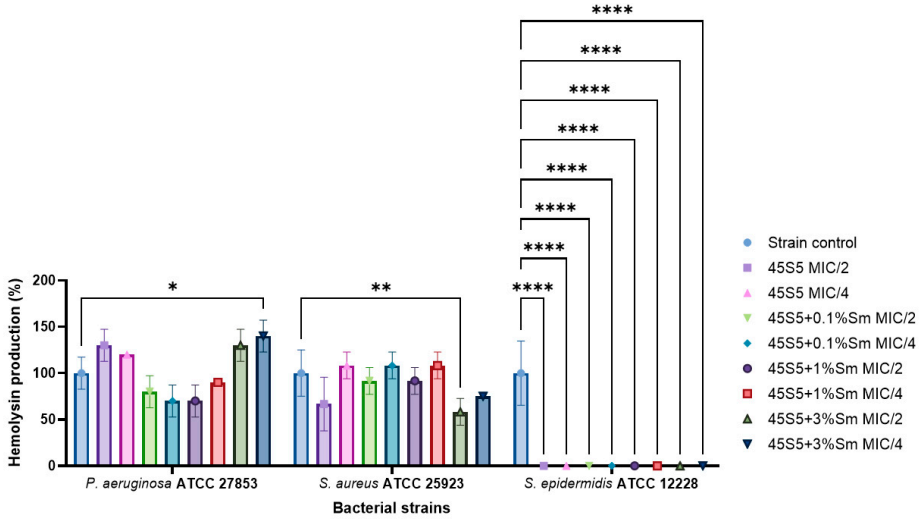

Figure 21. Graphic representation of the inhibitory effect of bioactive glass doped with Samarium on the ability of bacterial strains to produce hemolysin (* $p < 0.05$, ** $p < 0.01$; **** $p < 0.0001$).

The impact of the tested compounds on aesculin hydrolysis was evaluated in bacterial strains, including *K. pneumoniae* ATCC 13368, *S. aureus* ATCC 25923, and *S. epidermidis*

ATCC 12228. In the case of *S. epidermidis* ATCC 12228, a complete inhibition of aesculin hydrolysis (0%) was observed. Conversely, bioactive glass doped with samarium significantly enhanced aesculin hydrolysis in *K. pneumoniae* ATCC 13368, with increases ranging from 146% to 307%. The most pronounced effect was recorded for the 45S5 bioglass containing 1% Sm at a concentration of MIC/2, highlighting its strong stimulatory effect on this metabolic activity (Figure 22).

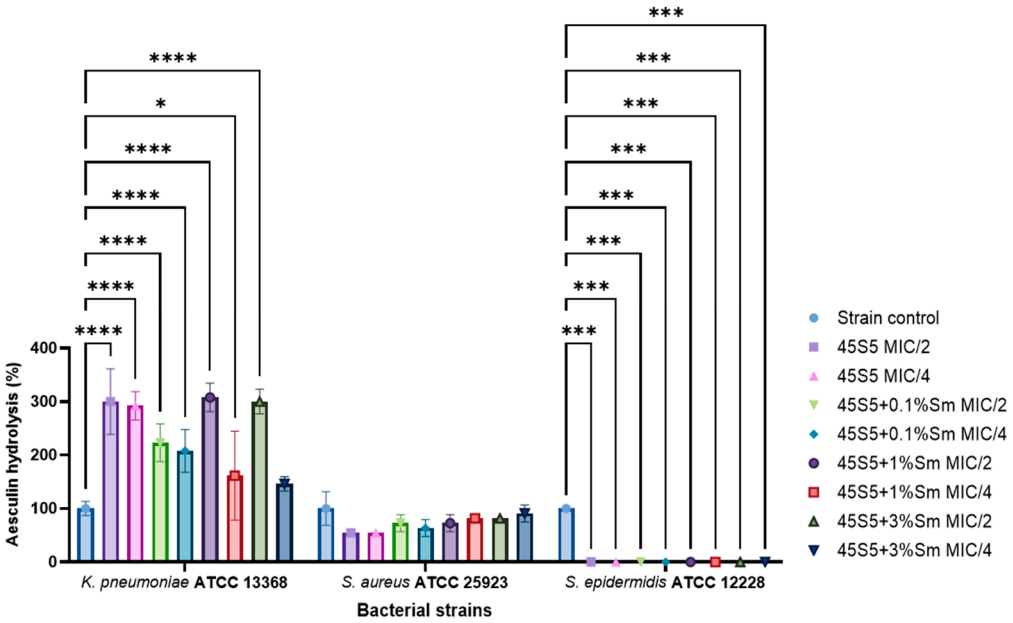

Figure 22. Graphic representation of the inhibitory effect of bioactive glass doped with Samarium on the ability of bacterial strains to hydrolyse aesculin (* $p < 0.05$, *** $p < 0.001$, **** $p < 0.0001$).

Lecithinase production was generally decreased for the *P. aeruginosa* ATCC 27853, *A. baylyi* ATCC 33305, *S. aureus* ATCC 25923, and *S. epidermidis* ATCC 12228 strains upon exposure to the tested samples, with percentages below 88.88%. However, in contrast to this overall trend, 45S5 bioglass at MIC/4 exhibited a stimulatory effect on soluble virulence factor production. Specifically, lecithinase activity increased to 116.66% in *P. aeruginosa* ATCC 27853 and 122.22% in *A. baylyi* ATCC 33305, indicating a concentration-dependent modulation of virulence-associated metabolic activities by 45S5 bioglass in certain strains (Figure 23).

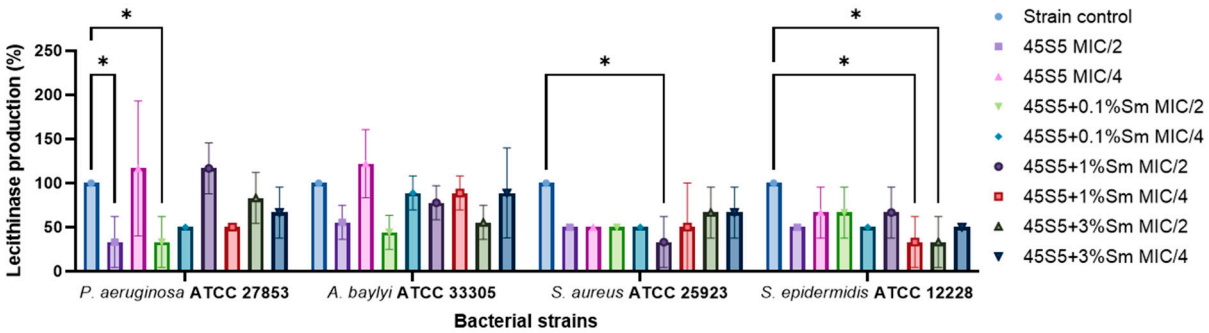

Figure 23. Graphic representation of the inhibitory effect of bioactive glass doped with Samarium on the ability of bacterial strains to produce lecithinase (* $p < 0.05$).

In the case of caseinase production, the capacity of the tested strains was stimulated after the treatment with all the samples. However, for *E. coli* ATCC 13846, a significant inhibition was registered at contact with 45S5 + 1% Sm MIC/4 (26.66%) (Figure 24).

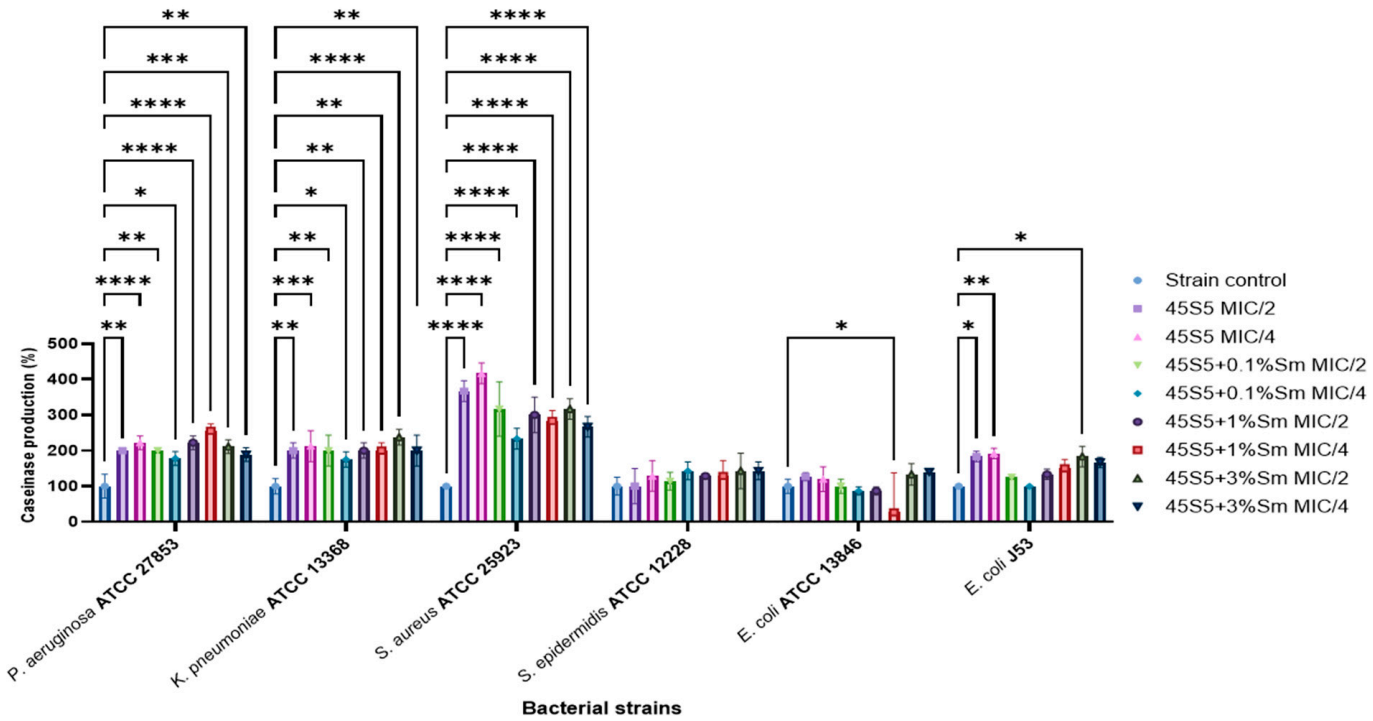

Figure 24. Graphic representation of the inhibitory effect of bioactive glass doped with Samarium on the ability of bacterial strains to produce caseinase (* $p < 0.05$, ** $p < 0.01$; *** $p < 0.001$, **** $p < 0.0001$).

Lipase production was inhibited in *A. baylyi* ATCC 33305 and *E. coli* ATCC 13846, with activity levels reduced to below 47%. In contrast, a significant stimulatory effect was observed in *S. epidermidis* ATCC 12228, with activity levels increasing substantially, ranging between 130% and 170%. This highlights a strain-specific response to the tested compounds, demonstrating their potential to differentially modulate enzymatic activity depending on the bacterial species (Figure 25).

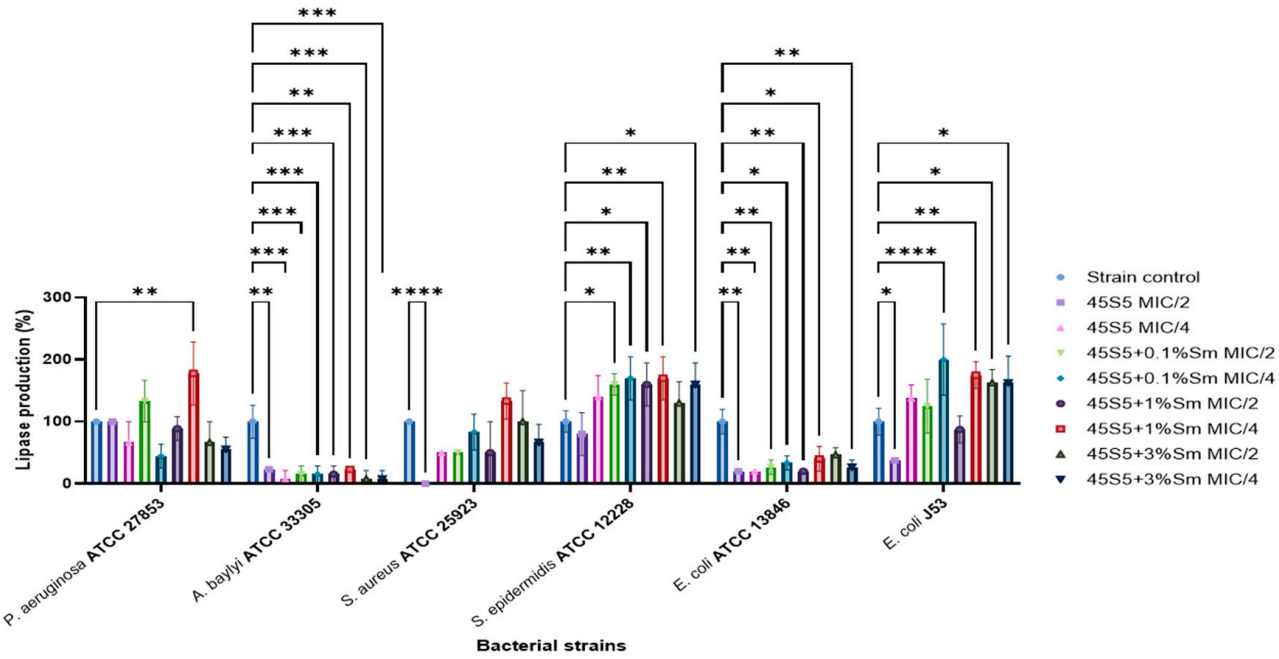

Figure 25. Graphic representation of the inhibitory effect of bioactive glass doped with Samarium on the ability of bacterial strains to produce lipase (* $p < 0.05$, ** $p < 0.01$; *** $p < 0.001$, **** $p < 0.0001$).

4. Conclusions

Samarium is a doping agent that is less studied and there are limited references in the literature that mention this element in combination with bioactive glasses. In this study, bioactive glasses doped with 0.1, 1.0, and 3.0% wt. of samarium were successfully prepared by the sol–gel method. The non-porous bioactive glass obtained through this method demonstrated bioactivity in vitro, with apatite formation occurring immediately and becoming visible within one day, as confirmed by both FTIR and X-ray diffraction. The results obtained after the characterization of the samples of bioactive glass doped with samarium indicated that this biomaterial presents good perspectives for biomedical applications. High cell density and good biocompatibility were generally observed in contact with Sm-enriched 45S5 bioactive glasses, even in the presence of 3.0% Sm. Although the antimicrobial activity of the 45S5 bioactive glass doped with samarium was generally limited, significant efficacy was observed against *A. baylyi* ATCC 33305 and *S. epidermidis* ATCC 12228. Additionally, all tested BG samples significantly reduced bacterial adherence in *S. aureus* ATCC 25923. The observed variability in virulence factor production underscores the material's potential for targeted biomedical applications. Thus, the bioactive glass doped with 0.1% Sm maintains cell viability but has limited antimicrobial activity. The addition of 1% Sm results in a material that is well-balanced in terms of biocompatibility and antimicrobial activity and can be considered the optimal concentration for general applications. Bioactive glass doped with 3% Sm is well-suited for applications necessitating enhanced antimicrobial control, albeit with a potential trade-off in long-term biocompatibility.

These findings lay the groundwork for further development of samarium-doped bioactive glass, with future studies focusing on in vivo testing and the incorporation of specific active agents to enhance bone regeneration and expand their therapeutic applications.

Author Contributions: Conceptualization, M.V.M. and A.F.; formal analysis, M.V.M., L.M., O.C.O., R.D.T., L.-R.B., R.P., A.Ș.D., V.M.C., V.-A.S., G.V., A.F., S.D. and I.G.-B.; investigation M.V.M., O.C.M., L.M., D.F., O.C.O., R.D.T., L.-R.B., R.P., A.Ș.D., V.M.C., V.-A.S., G.V., S.D. and I.G.-B.; writing—original draft, M.V.M., O.C.M., D.F., O.C.O., V.-A.S., G.V., A.F., S.D. and I.G.-B.; writing—review & editing, O.C.M., D.F., O.C.O., V.-A.S., G.V., A.F., S.D. and I.G.-B.; supervision, A.F. All authors have read and agreed to the published version of the manuscript.

Funding: This work was supported by the PN 23.06 Core Program—ChemNewDeal within the National Plan for Research, Development and Innovation 2022–2027, developed with the support of Ministry of Research, Innovation, and Digitization, project no. PN 23.06.02.01 (InteGral).

Institutional Review Board Statement: Not applicable.

Informed Consent Statement: Not applicable.

Data Availability Statement: Data are contained within the article.

Acknowledgments: The authors are grateful to the Romanian Government for providing access to the research infrastructure of the National Center for Micro and Nanomaterials through the National Program titled Installations and Strategic Objectives of National Interest-IOSIN.

Conflicts of Interest: M.V. Maximov and O.C. Maximov were employed by the company Microsin. The remaining authors declare that the research was conducted in the absence of any commercial or financial relationships that could be construed as a potential conflict of interest.

References

1. Hench, L.L.; Splinter, R.J.; Allen, W.C. Bonding Mechanisms at the Interface of Ceramic Prosthetic Materials. *J. Biomed. Mater. Res. Symp.* **1971**, *2*, 117–141.
2. Mîrt, A.-L.; Ficai, D.; Oprea, O.-C.; Vasilievici, G.; Ficai, A. Current and Future Perspectives of Bioactive Glasses as Injectable Material. *Nanomaterials* **2024**, *14*, 1196. [CrossRef]

3. Park, S.J.; Heogh, W.; Yang, J.; Kang, S.; Jeong, W.; Lee, H.; Jang, T.S.; Jung, H.D.; Jahazi, M.; Han, S.C.; et al. Meta-structure of amorphous-inspired 65.1Co28.2Cr5.3Mo lattices augmented by artificial intelligence. *Adv. Compos. Hybrid Mater.* **2024**, *7*, 224. [CrossRef]
4. Negut, I.; Ristoscu, C.; Tozar, T.; Dinu, M.; Parau, A.C.; Grumezescu, V.; Hapenciuc, C.; Popa, M.; Stan, M.S.; Mihailescu, I.N.; et al. Implant Surfaces Containing Bioglasses and Ciprofloxacin as Platforms for Bone Repair and Improved Resistance to Microbial Colonization. *Pharmaceutics* **2022**, *14*, 1175. [CrossRef]
5. Fiume, E.; Migneco, C.; Verné, E.; Baino, F. Comparison between Bioactive Sol-Gel and Melt-Derived Glasses/Glass-Ceramics Based on the Multicomponent SiO_2–P_2O_5–CaO–MgO–Na_2O–K_2O System. *Materials* **2020**, *13*, 540. [CrossRef]
6. Rizwan, M.; Hamdi, M.; Basirun, W.J. Bioglass® 45S5-based composites for bone tissue engineering and functional applications. *J. Biomed. Mater. Res. Part A* **2017**, *105*, 3197–3223. [CrossRef] [PubMed]
7. Porwal, H.; Grasso, S.; Cordero-Arias, L.; Boccaccini, A.R.; Li, C.; Reece, M.J. Processing and bioactivity of 45S5 Bioglass®-graphene nanoplatelets composites. *J. Mater. Sci. Mater. Med.* **2014**, *25*, 1403–1413. [CrossRef]
8. Xynos, I.D.; Edgar, A.J.; Buttery, L.D.K.; Hench, L.L.; Polak, J.M. Gene-expression profiling of human osteoblasts following treatment with the ionic products of Bioglass 45S5 dissolution. *J. Biomed. Mater. Res.* **2001**, *55*, 151–157. [CrossRef] [PubMed]
9. Morais, D.S.; Coelho, J.; Ferraz, M.P.; Gomes, P.S.; Fernandes, M.H.; Hussain, N.S.; Santosa, J.D.; Lopesa, M.A. Samarium doped glass-reinforced hydroxyapatite with enhanced osteoblastic performance and antibacterial properties for bone tissue regeneration. *J. Mater. Chem. B* **2014**, *2*, 5872. [CrossRef]
10. Pantulap, U.; Arango-Ospina, M.; Boccaccini, A.R. Bioactive glasses incorporating less-common ions to improve biological and physical properties. *J. Mater. Sci. Mater. Med.* **2022**, *33*, 3. [CrossRef]
11. Chellan, P.; Sadler, P.J. The elements of life and medicines. *Phil. Trans. R. Soc. A* **2015**, *373*, 20140182. [CrossRef] [PubMed]
12. Baranowska, A.; Kochanowicz, M.; Żmojda, J.; Miluski, P.; Wajda, A.; Leśniak, M.; Dorosz, D. Biological properties of rare-earth doped bioactive glass. *Opt. Fibers Their Appl.* **2020**, *11456*, 10. [CrossRef]
13. Iconaru, S.L.; Groza, A.; Gaiaschi, S.; Rokosz, K.; Raaen, S.; Ciobanu, S.C.; Chapon, P.; Predoi, D. Antimicrobial Properties of Samarium Doped Hydroxyapatite Suspensions and Coatings. *Coatings* **2020**, *10*, 1124. [CrossRef]
14. Balas, M.; Badea, M.A.; Ciobanu, S.C.; Piciu, F.; Iconaru, S.L.; Dinischiotu, A.; Predoi, D. Biocompatibility and Osteogenic Activity of Samarium-Doped Hydroxyapatite—Biomimetic Nanoceramics for Bone Regeneration Applications. *Biomimetics* **2024**, *9*, 309. [CrossRef]
15. Lavric, R.; Vreme, C.; Busuioc, C.; Isopencu, G.-O.; Nicoara, A.-I.; Oprea, O.-C.; Banciu, D.-D.; Constantinoiu, I.; Musat, A.-M.-R. The Effect of Silver and Samarium on the Properties of Bioglass Coatings Produced by Pulsed Laser Deposition and Spin Coating. *J. Funct. Biomater.* **2023**, *14*, 560. [CrossRef]
16. Zhang, Y.; Wang, X.; Su, Y.; Chen, D.; Zhong, W. A doxorubicin delivery system: Samarium/mesoporous bioactive glass/alginate composite microspheres. *Mater. Sci. Eng. C* **2016**, *67*, 205–213. [CrossRef]
17. Roberto, W.S.; Pereira, M.M.; Campos, T.P.R. Dosimetric Analysis and Characterization of Radioactive Seeds Produced by the Sol-Gel Method. *Key Eng. Mater.* **2003**, *240–242*, 579–582. [CrossRef]
18. Roberto, W.S.; Pereira, M.M.; Campos, T.P.R. Structure and Dosimetric Analysis of Biodegradable Glasses for Prostate Cancer Treatment. *Artif. Organs* **2003**, *27*, 432–436. [CrossRef]
19. Valente, E.S.; Campos, T.P.R. Gamma spectrometry and chemical characterization of ceramic seeds with samarium-153 and holmium-166 for brachytherapy proposal. *Appl. Radiat. Isot.* **2010**, *68*, 2157–2162. [CrossRef]
20. Maini, C.L.; Bergomi, S.; Romano, L.; Sciuto, R. 153Sm-EDTMP for bone pain palliation in skeletal metastases. *Eur. J. Nucl. Med. Mol. Imaging* **2004**, *31*, 171–178. [CrossRef]
21. Lam, M.G.E.H.; Dahmane, A.; Stevens, W.H.M.; Rijk, P.P.v.; Klerk, J.M.H.d.; Zonnenberg, B.A. Combined use of zoledronic acid and 153Sm-EDTMP in hormone-refractory prostate cancer patients with bone metastases. *Eur. J. Nucl. Med. Mol. Imaging* **2008**, *35*, 756–765. [CrossRef]
22. Kokubo, T.; Takadama, H. How useful is SBF in predicting in vivo bone bioactivity? *Biomaterials* **2006**, *27*, 2907–2915. [CrossRef] [PubMed]
23. Corbu, V.M.; Georgescu, A.-M.; Marinas, I.C.; Pericleanu, R.; Mogos, D.V.; Dumbravă, A.Ș.; Marinescu, L.; Pecete, I.; Vassu-Dimov, T.; Barbu, I.C.; et al. Phenotypic and Genotypic Characterization of Resistance and Virulence Markers in *Candida* spp. Isolated from Community-Acquired Infections in Bucharest, and the Impact of AgNPs on the Highly Resistant Isolates. *J. Fungi* **2024**, *10*, 563. [CrossRef] [PubMed]
24. Corbu, V.M.; Gheorghe, I.; Marinaș, I.C.; Geană, E.I.; Moza, M.I.; Csutak, O.; Chifiriuc, M.C. Demonstration of Allium sativum Extract Inhibitory Effect on Biodeteriogenic Microbial Strain Growth, Biofilm Development, and Enzymatic and Organic Acid Production. *Molecules* **2021**, *26*, 7195. [CrossRef]
25. Georgescu, M.; Gheorghe, I.; Curutiu, C.; Lazar, V.; Bleotu, C.; Chifiriuc, M.-C. Virulence and resistance features of Pseudomonas aeruginosa strains isolated from chronic leg ulcers. *BMC Infect. Dis.* **2016**, *16*, 92. [CrossRef]

26. Trușcă, B.S.; Gheorghe-Barbu, I.; Manea, M.; Ianculescu, E.; Barbu, I.C.; Măruțescu, L.G.; Dițu, L.-M.; Chifiriuc, M.-C.; Lazăr, V. Snapshot of Phenotypic and Molecular Virulence and Resistance Profiles in Multidrug-Resistant Strains Isolated in a Tertiary Hospital in Romania. *Pathogens* **2023**, *12*, 609. [CrossRef]
27. Gheorghe-Barbu, I.; Corbu, V.M.; Vrancianu, C.O.; Marinas, I.C.; Popa, M.; Dumbravă, A.Ș.; Niță-Lazăr, M.; Pecete, I.; Muntean, A.A.; Popa, M.I.; et al. Phenotypic and Genotypic Characterization of Recently Isolated Multidrug-Resistant Acinetobacter baumannii Clinical and Aquatic Strains and Demonstration of Silver Nanoparticle Potency. *Microorganisms* **2023**, *11*, 2439. [CrossRef]
28. Gavinho, S.R.; Graça, M.P.F.; Prezas, P.R.; Kumar, J.S.; Melo, B.M.G.; Sales, A.J.M.; Almeida, A.F.; Valente, M.A. Structural, thermal, morphological and dielectric investigations on 45S5 glass and glass-ceramics. *J. Non-Cryst. Solids* **2021**, *562*, 120780. [CrossRef]
29. Lefebvre, L.; Chevalier, J.; Gremillard, L.; Zenati, R.; Thollet, G.; Bernache-Assolant, D.; Govin, A. Structural transformations of bioactive glass 45S5 with thermal treatments. *Acta Mater.* **2007**, *55*, 3305–3313. [CrossRef]
30. Mecca, F.G.; Bellucci, D.; Cannillo, V. Effect of Thermal Treatments and Ion Substitution on Sintering and Crystallization of Bioactive Glasses: A Review. *Materials* **2023**, *16*, 4651. [CrossRef]
31. Pirayesh, H.; Nychka, J.A. Sol–Gel Synthesis of Bioactive Glass-Ceramic 45S5 and its in vitro Dissolution and Mineralization Behavior. *J. Am. Ceram. Soc.* **2013**, *96*, 1643–1650. [CrossRef]
32. Lombardi, M.; Gremillard, L.; Chevalier, J.; Lefebvre, L.; Cacciotti, I.; Bianco, A.; Montanaro, L. A Comparative Study between Melt-Derived and Sol-Gel Synthesized 45S5 Bioactive Glasses. *Key Eng. Mater.* **2013**, *541*, 15–30. [CrossRef]
33. Faure, J.; Drevet, R.; Lemelle, A.; Jaber, N.B.; Tara, A.; Btaouri, H.E.; Benhayoune, H. A new sol–gel synthesis of 45S5 bioactive glass using an organic acid as catalyst. *Mater. Sci. Eng. C* **2015**, *47*, 407–412.
34. Hum, J.; Boccaccini, A.R. Collagen as Coating Material for 45S5 Bioactive Glass-Based Scaffolds for Bone Tissue Engineering. *Int. J. Mol. Sci.* **2018**, *19*, 1807. [CrossRef]
35. Ohsato, H.; Maki, I.; Takéuchi, Y. Structure of $Na_2CaSi_2O_6$. *Acta Crystallogr. Sect. C Struct. Chem.* **1985**, *41*, 1575–1577. [CrossRef]
36. Ihara, M.; Odani, K.; Yoshida, N.; Fukunaga, J.; Setoguchi, M.; Higashi, T. The crystal Stucture of Devitrite (Disodium Tricalcium Hexasilicate) $Ca_3Na_2Si_6O_{16}$. *J. Ceram. Assoc. Jpn.* **1984**, *92*, 373–378. [CrossRef]
37. Wilson, R.M.; Elliott, J.C.; Dowker, S.E.P. Rietveld refinement of the crystallographic structure of human dental enamel apatites. *Am. Miner.* **1999**, *84*, 1406–1414. [CrossRef]
38. Ershad, M.; Vyas, V.K.; Prasad, S.; Ali, A.; Pyare, R. Effect of Sm_2O_3 substitution on mechanical and biological properties of 45S5 bioactive glass. *J. Aust. Ceram. Soc.* **2018**, *54*, 621–630. [CrossRef]
39. Wu, C.; Chang, J. Mesoporous bioactive glasses: Structure characteristics, drug/growth factor delivery and bone regeneration application. *Interface Focus* **2012**, *2*, 292–306. [CrossRef]
40. Ungureanu, D.N.; Angelescu, N.; Tsakiris, V.; Marinescu, V. Investigations regarding chemical synthesis of calcium hydroxyapatite. *Rom. J. Mater.* **2012**, *42*, 52–60.
41. Maximov, M.; Maximov, O.-C.; Craciun, L.; Ficai, D.; Ficai, A.; Andronescu, E. Bioactive Glass—An Extensive Study of the Preparation and Coating Methods. *Coatings* **2021**, *11*, 1386. [CrossRef]
42. Nica, I.C.; Popa, M.; Marutescu, L.; Dinischiotu, A.; Iconaru, S.L.; Ciobanu, S.C.; Predoi, D. Biocompatibility and Antibiofilm Properties of Samarium Doped Hydroxyapatite Coatings: An In Vitro Study. *Coatings* **2021**, *11*, 1185. [CrossRef]
43. Araujo, M.S.; Silva, A.C.; Cabal, B.; Bartolomé, J.F.; Mello-Castanho, S. In vitro bioactivity and antibacterial capacity of 45S5 Bioglass®-based compositions containing alumina and strontium. *J. Mater. Res. Technol.* **2021**, *13*, 154–161. [CrossRef]
44. Hammami, I.; Gavinho, S.R.; Jakka, S.K.; Valente, M.A.; Graça, M.P.F.; Pádua, A.S.; Silva, J.C.; Sá-Nogueira, I.; Borges, J.P. Antibacterial Biomaterial Based on Bioglass Modified with Copper for Implants Coating. *J. Funct. Biomater.* **2023**, *14*, 369. [CrossRef] [PubMed]
45. Zhang, C.; Ru, Y.; You, J.; Lin, R.; Chen, S.; Qi, Y.; Li, D.; Zhang, C.; Qiu, Z. Antibacterial Properties of PCL@45s5 Composite Biomaterial Scaffolds Based on Additive Manufacturing. *Polymers* **2024**, *16*, 3379. [CrossRef]
46. Yan, X.; Zhang, F.; Ding, M.; Xiang, L.; Bai, J.; Li, Q.; Zhou, Y. Klebsiella pneumoniae BolA contributes to cell morphology, siderophore production, stresses challenge, cell adhesion and virulence. *bioRxiv* **2021**. [CrossRef]
47. Zhou, P.; Garcia, B.L.; Kotsakis, G.A. Comparison of antibacterial and antibiofilm activity of bioactive glass compounds S53P4 and 45S5. *BMC Microbiol.* **2022**, *22*, 212. [CrossRef]